ORGANOMETALLICS

pubs.acs.org/Organometallics

Article

# Nickel-Catalyzed Alkyne Cyclotrimerization Assisted by a Hemilabile Acceptor Ligand: A Computational Study

Alessio F. Orsino and Marc-Etienne Moret*

Cite This: *Organometallics* 2020, 39, 1998–2010

Read Online

ACCESS | Metrics & More | Article Recommendations | Supporting Information

**ABSTRACT:** $\pi$-coordinating units incorporated in the supporting ligand of an organometallic complex may open up specific reactive pathways. The diphosphine ketone supported nickel complex [($^{p\text{-tol}}$**L1**)Ni(BPI)] ($^{p\text{-tol}}$**1**; $^{p\text{-tol}}$**L1** = 2,2′-bis(di-*p*-tolylphosphino)-benzophenone; BPI = benzophenone imine) has previously been shown to act as an active and selective alkyne cyclotrimerization catalyst. Herein, DFT calculations support an adaptive behavior of the ligand throughout the catalytic cycle, several elementary steps being assisted by coordination or decoordination of the C═O moiety. A comparison with related bi- and tridentate phosphine ligands reveals the key role of the hemilabile $\pi$-acceptor moiety for the catalytic activity and selectivity of $^{p\text{-tol}}$**1** in alkyne cyclotrimerization.

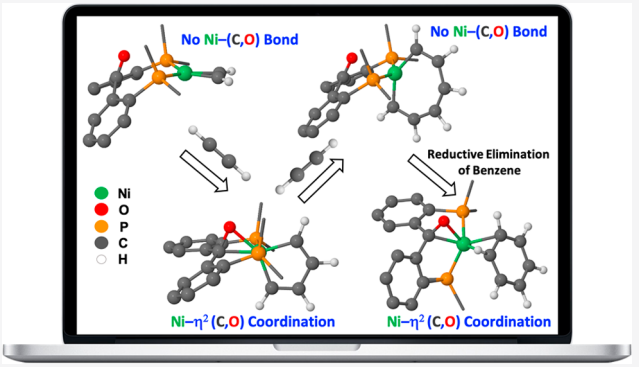


## INTRODUCTION

The development of efficient and sustainable methodologies for the formation of carbon−carbon bonds has always been a central topic in synthetic chemistry. In particular, the metal-catalyzed [2 + 2 + 2] cycloaddition of alkynes is a powerful and versatile protocol in the construction of functionalized ring systems.[1] The transformation is suitable for a variety of unsaturated motifs, allowing for the construction of various substituted six-membered cycles, such as benzenes, pyridines, and 1,3-cyclohexadienes. Such polysubstituted arenes are at the core of many natural products and are attractive synthetic targets for both industry and academia.[2] The catalytic cyclotrimerization of alkynes has been intensely studied, which has resulted in the development of a number of metal-based catalytic systems.

Since the initial reports of Reppe et al. in the Ni-catalyzed cyclooligomerization of alkynes, describing in two separate papers both the formation of cyclooctatetraene (COT)[3] and substituted benzenes,[4] the cyclotrimerization of alkynes mediated by nickel complexes has been extensively investigated (see Chart 1 for selected examples).[5] Early contributions in the field include investigations reported by the Eisch group about the transformation of internal alkynes with phosphine-supported nickelacylopentadienes to lead to the formation of polysubstituted benzenes (Chart 1A; top left).[6] Pörschke and co-workers extensively studied the reaction of acetylene with phosphine-based and diazadiene-based nickel complexes, which provided insights into the structure of certain catalytic intermediates in Ni-catalyzed cyclotrimerization reactions (Chart 1A, top right, and Chart 1B, right).[7] In 2013, the Guan group reported an easily accessible and highly efficient *in*

**Chart 1. Nickel Systems for Alkyne Cyclotrimerization Reactions**[a]

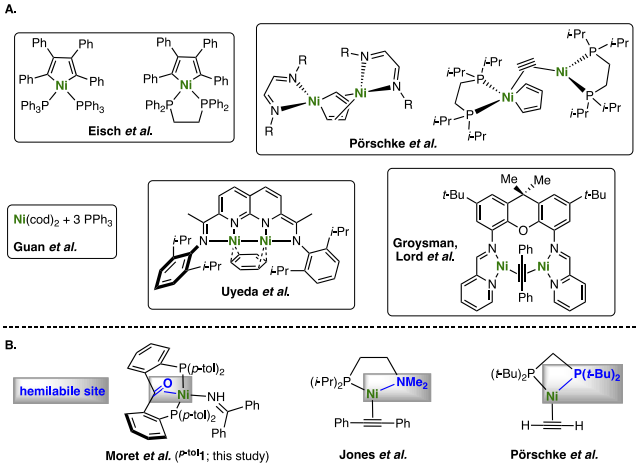


[a](A) Selected examples of representative Ni systems for alkyne cyclotrimerization, separated by research group;[6−10] R = 1,3-diisopropylbenzene. (B) Examples of mechanistic studies on mononuclear Ni(0) complexes in which a metal−ligand adaptive mechanism was proposed.[7d,e,13,21c]

**Received:** March 10, 2020
**Published:** May 13, 2020









https://dx.doi.org/10.1021/acs.organomet.0c00172
*Organometallics* 2020, 39, 1998–2010

*situ* generated Ni system ($Ni(cod)_2$ + 3 equiv of $PPh_3$), active and regioselective for a wide range of ynoates and other related alkynes, with a TON as high as 2000 for the cyclotrimerization of ethyl propiolate at room temperature and within 2 h (Chart 1A, bottom left).[8] Recently, the dinickel complexes from the Uyeda group[9] and the Groysman and Lord groups[10] were shown to promote the regio- and chemoselective cyclotrimerization of several terminal alkynes, preferentially forming the 1,2,4-trisubstituted arenes over the substituted COT products and outperforming related mononuclear Ni complexes of N-bound-containing ligands and $Ni(cod)_2$, for which cyclotetramerization is generally favored (Chart 1A, bottom right).

Our group recently reported the use of a hemilabile ligand featuring an electron-accepting $\pi$ ligand as a labile moiety,[11] 2,2′-bis(di-*p*-tolylphosphino)benzophenone ($^{p\text{-tol}}$**L1**),[12] for alkyne cyclotrimerization (Chart 1B, left).[13] The Ni(0) complex [($^{p\text{-tol}}$**L1**)Ni(BPI)] ($^{p\text{-tol}}$**1**; BPI = benzophenone imine) was shown to be an active catalyst for terminal alkyne cyclotrimerization, selectively affording the 1,2,4-trisubstituted arene product over the 1,3,5-isomer and larger rings such as COTs. The results obtained with $^{p\text{-tol}}$**1** contrasted with those of the tridentate trisphosphine [($^{p\text{-tol}}$**L2**)Ni(BPI)] ($^{p\text{-tol}}$**2**; $^{p\text{-tol}}$**L2** = bis[2-(di-*p*-tolylphosphino]phenyl]phenylphosphine and the bidentate diphosphine ether [($^{Ph}$**L3**)Ni(BPI)] ($^{Ph}$**3**; $^{Ph}$**L3** = bis[2-(diphenylphosphino)phenyl] ether) complexes. Namely, the tridentate ligand $^{p\text{-tol}}$**L2** afforded a considerably less active catalyst, while the bidentate $^{Ph}$**L3** resulted in both lower activity and lower selectivity for trimerization over tetramerization. The hemilabile behavior of $^{p\text{-tol}}$**1** was evidenced by the decoordination of the C═O moiety from $^{p\text{-tol}}$**1** upon exchange of the BPI ligand for alkynes to form the mono(alkyne) resting state. In addition, a preliminary DFT study showed that the C═O bond is bound to Ni in the key metallacyclopentadiene intermediate (see Scheme 1 for the commonly proposed mechanism).

The mechanism of the transition-metal-catalyzed cyclotrimerization of alkynes has been the subject of several experimental and computational studies.[14] The generally accepted pathway from the mono(alkyne) complex **I** first involves the oxidative coupling of two alkynes **II** to yield the metallacyclopentadiene **IIIa** or its biscarbene resonance structure **IIIb**, commonly proposed to be rate determining (Scheme 1; see section 1.1 in the Supporting Information for a more detailed picture of the mechanism).[15] The generated metallacycle is a key intermediate for both activity and regioselectivity (i.e., ratio between the 1,2,4- and 1,3,5-trisubstitued isomers; see also section 1.2 in the Supporting Information). Subsequently, the insertion of the third alkyne to form the final aromatic product can proceed via a [4 + 2] (**IV** or **V**) or [2 + 2] (**VI**) cycloaddition pathway or through the migratory insertion (**VII**) of the alkyne into a metal−carbon bond.[1h] This final step likely governs the selectivity of the cyclotrimerized product vs larger-size rings (mostly cyclooctatetraenes)[16] or oligomers and may also influence the regioselectivity. A $\pi$-bound benzene adduct (**VIII**) is commonly proposed along the cycle, prior to the liberation of the cyclotrimerized product and the regeneration of the mono(alkyne) intermediate **I**. Some examples of mechanistically well studied systems include cyclopentadiene (Cp)-supported cobalt[17] and ruthenium,[18] in addition to rhodium-based systems with different types of ligands.[19]

**Scheme 1. Simplified Commonly Proposed Catalytic Cycle for the Metal-Catalyzed Cyclotrimerization of Acetylene into Benzene**[14, a]

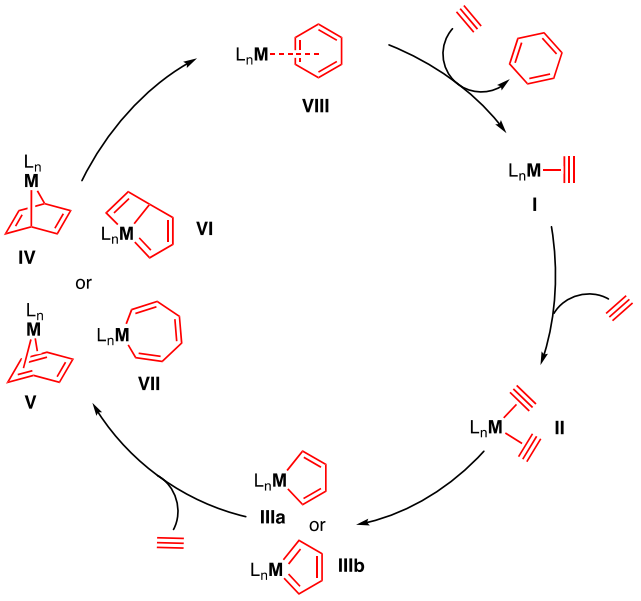


[a]The addition of the third molecule of acetylene can also occur stepwise via an intermediate halt, with first coordination of acetylene to the metal (i.e., with a M−$\eta^2$-(HC≡CH) bond), prior to the new $\sigma$ C−C bond formation.

Mechanistic investigations on nickel catalysts are somewhat less common.[13,20,21] Two examples indicate the utility of hemilabile, bidentate ligands. First, Jones' nickel(0) complex of a hybrid phosphino-amino (PN) ligand (Chart 1B, middle) was shown to be significantly more active than complexes of the related diphosphine ligand (PP = 1,2-bis-(diisopropylphosphino)ethane),[21c] which was attributed to the ability of the weakly donating amine arm to free up a coordination site (section 1.3 and Figure S1 in the Supporting Information). Second, Pörschke and co-workers studied the stoichiometric cyclotrimerization of acetylene at a Ni(0) center supported by a bulky diphosphinomethylene ligand (Chart 1B, right) to form an $\eta^6$-bound benzene−Ni complex, in which only one P-donor atom is bound to Ni.[7d] This hemilabile behavior of the diphosphine ligand likely arises from the moderate stability of four-membered chelate rings (section 1.3 and Scheme S3 in the Supporting Information).[7e] Additionally, Uyeda,[9,21d] Ess,[21d] and Groysman and Lord[10] recently probed the mechanism of alkyne cyclotrimerizations catalyzed by dinuclear nickel bis(imino)pyridine catalysts (Chart 1A, bottom right). In both cases, the transformation was suggested to occur through a migratory insertion pathway for the incorporation of the third alkyne into the cyclotrimerized product, the bimetallic architectures preventing the insertion of the fourth equivalent of alkyne (section 1.3 and Figure S2 in the Supporting Information).

Here we report a DFT study of the potential energy surface for the cyclotrimerization of alkynes catalyzed by $^{p\text{-tol}}$**1** (Chart 1B, left) that accounts for the experimental observations. In particular, the role of the labile $\pi$-acceptor C═O unit throughout the reaction is investigated. The difference in activity and selectivity among the diphosphine ketone $^{p\text{-tol}}$**1**, trisphosphine $^{p\text{-tol}}$**2**, and diphosphine ether $^{Ph}$**3** complexes are also investigated by DFT calculations.


https://dx.doi.org/10.1021/acs.organomet.0c00172
Organometallics 2020, 39, 1998−2010

## RESULTS AND DISCUSSION

**General Considerations.** To assess the effect of the hemilabile C═O moiety from $^{p\text{-tol}}$**L1** in alkyne cyclotrimerization reactions and understand the differences in reactivity among $^{p\text{-tol}}$**1**, $^{p\text{-tol}}$**2**, and $^{Ph}$**3** observed experimentally, plausible mechanistic pathways were mapped by DFT calculations. The Gibbs free energies were obtained at $T$ = 298.15 K, from a M06L/def2TZVP single-point refinement with the toluene solvent model based on density (SMD) and dispersion correction (GD3) using the geometries optimized at the M06L-GD3/6-31g(d,p) level of theory and frequencies calculated at the same level (see also the Experimental Section for more details). Calculations were performed on a slightly truncated model system (phenyl substituents instead of *p*-tolyl on the phosphorus side arms; Chart 2A), using acetylene as the alkyne substrate (Chart 2B). The discussion starts with a general description of the Gibbs free energy surface calculated for the cyclotrimerization of acetylene into benzene catalyzed by $^{Ph}$**1** (Gibbs Free Energy Surface). Next, each elementary step is addressed in detail, describing the considered alternatives (from Alkyne Coordination Step to Regioselectivity). Finally, the geometric and energetic differences (or similarities) between the catalytic intermediates supported by $^{Ph}$**L1** and those containing the strong tridentate ligand $^{Ph}$**L2** and the bidentate ligand $^{Ph}$**L3** are investigated (Comparison with the Tridentate Trisphosphine and the Bidentate Diphosphine Ether Ligands).

**Chart 2. Ligands (A) and the Mono(acetylene) Ni Complexes (B) Used in This Study to Computationally Investigate the Ni-Catalyzed Cyclotrimerization of Terminal Alkynes, Using Catalysts $^{p\text{-tol}}$1, $^{p\text{-tol}}$2, and $^{Ph}$3**[a]

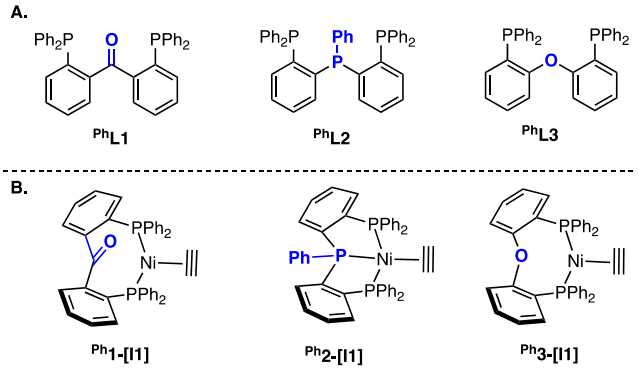


[a]"I" stands for intermediate.

**Gibbs Free Energy Surface.** Figure 1 depicts the calculated Gibbs free energy surface, including the intermediates and transition states involved in the cyclotrimerization of acetylene catalyzed by $^{Ph}$**1** in a singlet spin state. An overall exergonic $\Delta G^\circ$ value of −131.0 kcal/mol was calculated, in acceptable agreement with the experimental value of ca. −137 kcal/mol found for the cyclotrimerization of acetylene into benzene.[22] The proposed pathway is divided into distinct parts (i.e., alkyne coordination, oxidative coupling, second alkyne coordination, insertion, reductive elimination of benzene, and substrate exchange), which are detailed step by step in the next subsections. Overall, the alkyne coordination steps are endergonic ($\Delta G^\circ$ = +10.4 and +7.7 kcal/mol, respectively), while all of the other steps are favorable and exergonic. The coordinations of both the second and third acetylene molecules to Ni are slightly exothermic ($\Delta H^\circ$ = −0.7 and −2.9 kcal/mol, respectively); the entropic contributions ($T\Delta S^\circ$ = −11.1 and −10.5 kcal/mol, respectively), and hence the endergonicity of these elementary steps, are probably overestimated in the gas phase.

Remarkably, the ligand adapts its coordination geometry by reversible binding of the C═O moiety to Ni throughout the Gibbs free energy surface, stabilizing catalytic intermediates or transition states. Elementary steps such as alkyne coordination, oxidative coupling, reductive elimination, and substrate exchange are coupled to changes in the coordination of the ketone (see also section 2.3.1 and Table S2 in the Supporting Information for natural bond orbital analysis of the intermediates). Of particular importance, the rate-determining oxidative coupling step ($^{Ph}$**1**-[**I2**] → $^{Ph}$**1**-[**I3**]) is assisted by $\pi$ coordination of the C═O unit to Ni, which stabilizes the key metallacyclopentadiene intermediate. An overall energy barrier of $\Delta G^{\circ,\ddagger}$($^{Ph}$**1**-[**TS2**]) = +26.2 kcal/mol is in the acceptable range limit (∼25 kcal/mol)[23] for a reaction proceeding at room temperature: catalytic experiments proceed under nonstandard conditions (vs calculated under standard conditions), the alkyne substrate concentration being significantly greater than the concentration of the nickel species. The experimental activation Gibbs free energy of the rate-limiting step ($\Delta G^{\ddagger}$) is therefore expected to be lower than the activation Gibbs free energy computationally determined under standard conditions ($\Delta G^{\circ,\ddagger}$), as the nonstandard equation applies (i.e., $\Delta G = \Delta G^\circ + RT \ln Q$, with $R$ = gas constant and $Q$ = reaction quotient). In addition, the structure and geometry of $^{Ph}$**1**-[**TS2**] are likely determinant for the regioselectivity of the reaction when a substituted alkyne is used (see Regioselectivity for more details).

**Alkyne Coordination Step.** Bis(acetylene) complexes have often been proposed along transition-metal-catalyzed alkyne cyclotrimerization pathways. The monoalkyne resting state of the catalyst, $^{Ph}$**1**-[**I1**], adopts a tricoordinate, 16-VE configuration, with an unbound ketone ($C_{ke}$−O = 1.23 Å; Ni−$C_{ke}$ = 3.51 Å; Ni−O = 3.19 Å; ke = ketone), consistent with *in situ* experimental observations.[13] The transition state for the alkyne uptake, $^{Ph}$**1**-[**TS1**], has a Gibbs free energy of 13.9 kcal/mol relative to $^{Ph}$**1**-[**I1**] and is characterized by an imaginary frequency that corresponds to the $\eta^2$ bond formation between nickel and acetylene (Ni−$C_{ac}$ = 2.05 Å; Ni−$C_{ac}$ = 2.62 Å; ac = acetylene). This step is endergonic by 10.4 kcal/mol, to afford a tetracoordinate 18-VE bis(alkyne) intermediate, $^{Ph}$**1**-[**I2**], unsurprisingly devoid of a Ni−(C═O) interaction ($C_{ke}$−O = 1.24 Å; Ni−$C_{ke}$ = 3.42 Å; Ni−O = 3.02 Å). During this step (Figure 2), no significant changes in geometry or rehybridization of the C═O fragment are observed. In the optimized structure of $^{Ph}$**1**-[**I2**], the acetylene ligands are coordinated with elongated Ni−$C_{ac}$ (1.93−1.98 Å) distances in comparison to the mono(alkyne) analogue $^{Ph}$**1**-[**I1**] (1.84 Å), an effect that has been reported in other DFT studies.[17a,g,h]

Alternative pathways, involving decoordination of one phosphine arm from $^{Ph}$**L1**, have also been considered. Bis(acetylene) structures with Ni−$\eta^1$(O) or Ni−$\eta^2$(C,O) or without coordination of the ketone unit to Ni were not located; instead, geometry optimizations converged to $^{Ph}$**1**-[**I2**], excluding the involvement of such intermediates along the Gibbs free energy surface for this specific step.

**Oxidative Coupling Step.** From the bis(acetylene) complex $^{Ph}$**1**-[**I2**], several closed-shell or open-shell pathways have been considered for the coupling of two acetylene


https://dx.doi.org/10.1021/acs.organomet.0c00172
Organometallics 2020, 39, 1998−2010

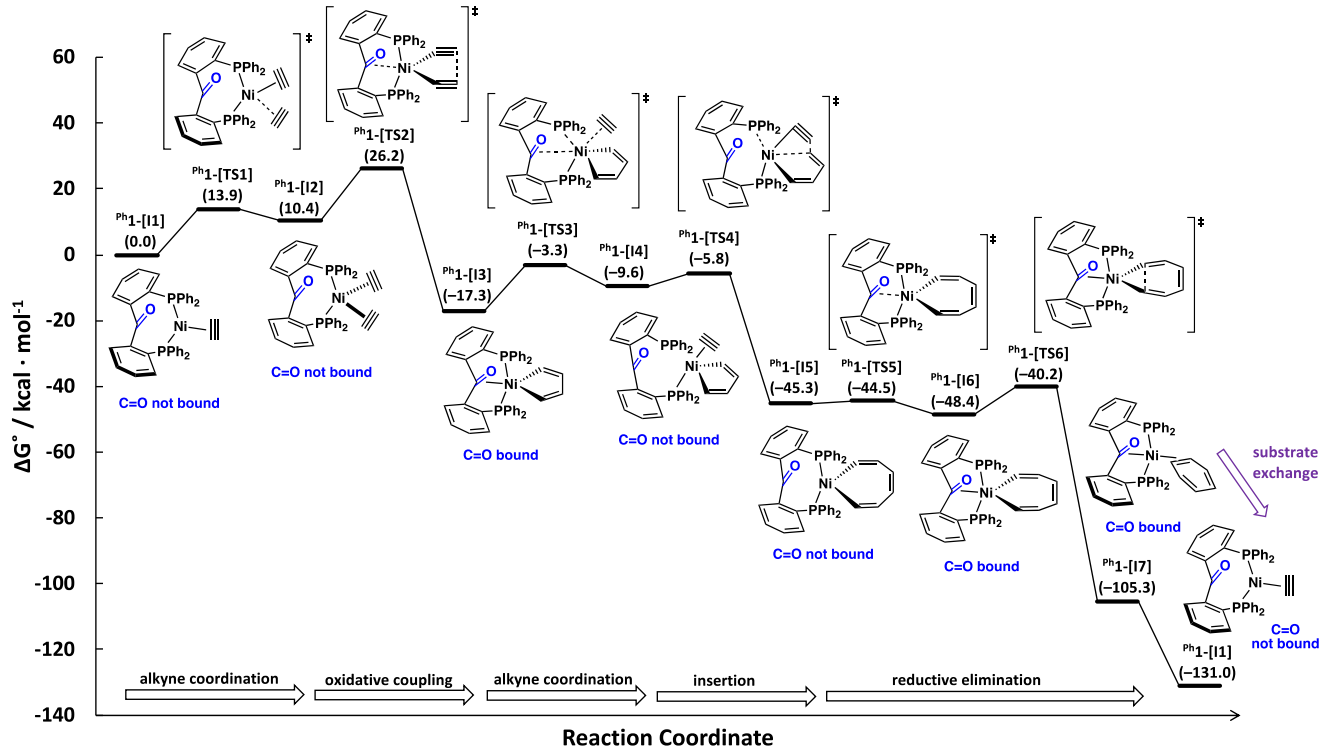


**Figure 1.** Calculated relative Gibbs free energies (in kcal/mol; M06L-GD3/def2TZVP/SMD//M06L-GD3/6-31g(d,p), $T$ = 298.15 K) for the cyclotrimerization of acetylene into benzene, starting from [($^{Ph}$**L1**)Ni(HC≡CH)] ($^{Ph}$**1**-[**I1**]), on the singlet spin state surface. For clarity, the free acetylene and benzene substrate molecules are not shown but have been accounted for in the energy calculations. Values in parentheses are Gibbs free energies in kcal/mol. Dotted lines in the illustration of the transition states represent bonds being formed or broken.

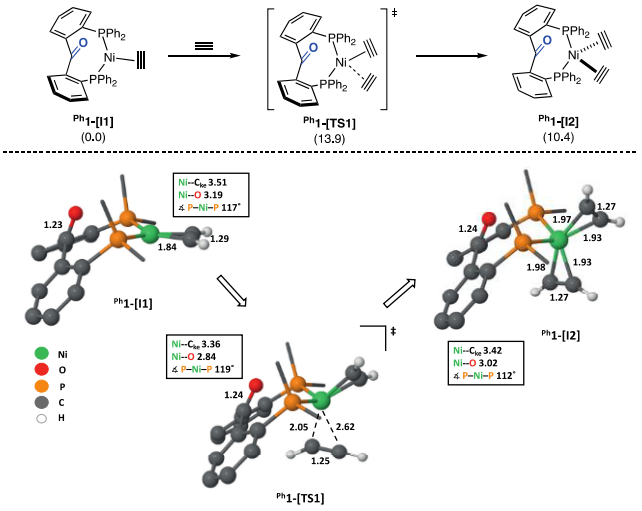


**Figure 2.** Acetylene coordination step on the singlet spin-state surface. (top) Schematic representation of the elementary step, with related Gibbs free energies given in kcal/mol (values in parentheses). (bottom) Optimized geometries (M06L-GD3/6-31g(d,p)) of the intermediates and transition states. Hydrogen atoms (except from the alkyne) and phenyl substituents on phosphorus arms have been omitted for clarity. Dotted lines in $^{Ph}$**1**-[**TS1**] represent a bond being formed. Bond lengths are given in Å.

fragments (Figure 3).[24] First, the most stable intermediate is the pentacoordinate metallacyclopentadiene $^{Ph}$**1**-[**I3**], arising from the oxidative coupling from $^{Ph}$**1**-[**I2**], with concerted formation of one $\sigma$(C−C) and two $\sigma$(Ni−C) bonds. $^{Ph}$**1**-[**I3**] adopts a trigonal-bipyramidal geometry in which the C═O moiety from $^{Ph}$**L1** is $\eta^2$ bound. The strong $\sigma$ donation from the bidentate hydrocarbyl ligand to Ni can be stabilized in the equatorial plane of the bipyramid by the $\pi$-accepting ketone unit, as revealed by elongation of the C−O bond (from 1.24 Å in $^{Ph}$**1**-[**I2**] to 1.36 Å). The $\pi$ electrons on the butadienyl ligand in $^{Ph}$**1**-[**I3**] are mostly localized between the $C_\alpha$ and $C_\beta$ positions, with little delocalization throughout the metallacycle.[25] Indeed, the calculated bond lengths of 1.35 and 1.46 Å respectively fall into the expected range for a pure C═C double bond, such as ethylene, and a $\sigma$ C−C bond between two sp$^2$-hybridized carbons.[26] This assignment is consistent with the metallacycle formation model proposed by Thorn and Hofmann in 1979, on the basis of Hückel theory, who described a nonoptimal overlap between the filled d orbitals of the metal and $\pi^*$ orbitals from the alkene,[27] this effect preventing the effective electronic delocalization throughout the metallacycle.

In addition to $^{Ph}$**1**-[**I3**], the putative zwitterionic intermediate $^{Ph}$**1**-[**I3**]' is located at 30.8 kcal/mol above $^{Ph}$**1**-[**I1**], significantly higher than the transition state $^{Ph}$**1**-[**TS2**], and hence can be ruled out. In comparison to the pentacoordinate intermediate $^{Ph}$**1**-[**I3**], the tetracoordinate analogues with a Ni−($\kappa^2$-(CO,P)) or Ni−($\kappa^2$-(P,P)) binding mode are both unfavorable. While the Ni−($\kappa^2$-(P,P)) species could not be found on the potential energy surface and its optimization always collapsed into $^{Ph}$**1**-[**I3**], the Ni−($\kappa^2$-(CO,P)) intermediate $^{Ph}$**1**-[**I3**]'' was calculated to be 4.2 kcal/mol higher in energy. In addition, a transition state leading to $^{Ph}$**1**-[**I3**]'' could not be located because its corresponding bis(alkyne) precursor, i.e., a Ni−($\kappa^2$-(CO,P)) bis(acetylene) species, was not detected on the potential energy surface (*vide supra*). Finally, the triplet structure of $^{Ph}$**1**-[**I3**] was also found to be 7.6 kcal/mol above the singlet configuration (section 2.3.1 and


https://dx.doi.org/10.1021/acs.organomet.0c00172
Organometallics 2020, 39, 1998−2010

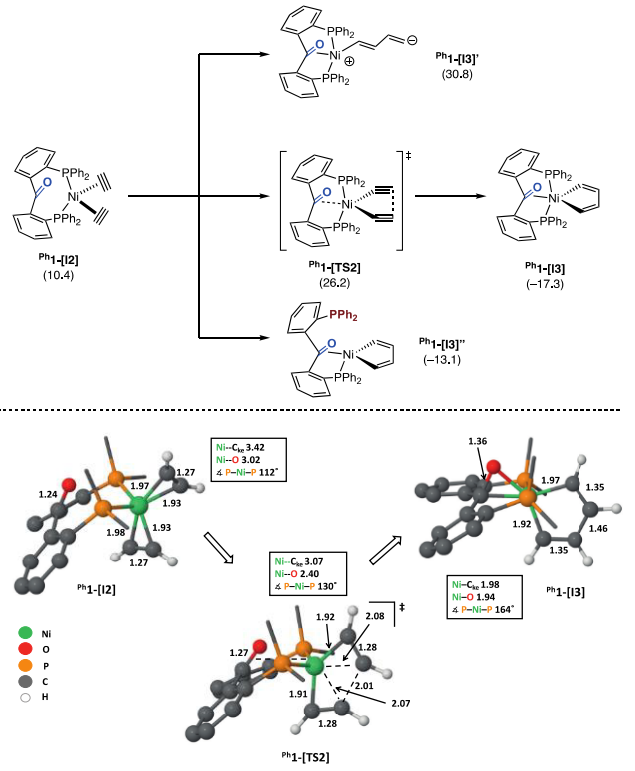


**Figure 3.** Oxidative coupling rate-determining step on the singlet spin-state surface. (top) Schematic representation of the elementary step, including different possible pathways, with related Gibbs free energies given in kcal/mol (values in parentheses). (bottom) Optimized geometries (M06L-GD3/6-31g(d,p)) of the intermediates and the transition state. Hydrogen atoms (except from the alkyne and hydrocarbyl ligands) and the phenyl substituents on the phosphorus arms have been omitted for clarity. The dotted lines in $^{Ph}$**1**-[**TS2**] represent bonds being formed or broken. Bond lengths are given in Å.

Figure S3 in the Supporting Information), rendering a two-state mechanism unlikely.

The oxidative coupling step from the bis(acetylene) complex $^{Ph}$**1**-[**2**] to MCP $^{Ph}$**1**-[**I3**] is exergonic by −27.7 kcal/mol (−17.3 kcal/mol relative to $^{Ph}$**1**-[**I1**]) with an energy barrier of +15.8 kcal/mol (+26.2 kcal/mol in respect to $^{Ph}$**1**-[**I1**]), for which the driving force is the formation of a new $\sigma$ C−C bond.[17a] In comparison with other elementary steps, the MCP formation from this system is found to be rate determining, in accord with reported DFT studies in alkyne cyclotrimerization mediated by other metal catalysts.[1,14]

The transition state $^{Ph}$**1**-[**TS2**] is characterized by a single imaginary vibrational frequency, corresponding to the formation of a new C−C $\sigma$ bond. A slight participation of the $\pi$-acceptor central C═O moiety in $^{Ph}$**1**-[**TS2**] is evident from the shortening of the Ni−O (3.02 Å in $^{Ph}$**1**-[**I2**] to 2.40 Å in $^{Ph}$**1**-[**TS2**]) and Ni−C (3.42 Å in $^{Ph}$**1**-[**I2**] to 3.07 Å in $^{Ph}$**1**-[**TS2**]) distances. The concomitant increase of the $C_{ke}$−O bond length from 1.24 Å in $^{Ph}$**1**-[**I2**] to 1.27 Å in $^{Ph}$**1**-[**TS2**] is indicative of some degree of $\pi$ interaction. The corresponding Wiberg bond indexes (WBIs) are in accord with this interpretation, with a WBI ($C_{ke}$−O) decrease from 1.59 ($^{Ph}$**1**-[**I2**]) to 1.45 ($^{Ph}$**1**-[**TS2**]) and 1.14 ($^{Ph}$**1**-[**I3**]) and with a slight overlap of the orbitals between Ni and C═O in $^{Ph}$**1**-[**TS2**] (WBI(Ni−O) = 0.11 and WBI(Ni−$C_{ke}$) = 0.10). The forming $\pi$ interaction is correlated with a change in the P−Ni−P angle from 112° in the bidentate state of $^{Ph}$**L1** ($^{Ph}$**1**-[**I2**]) to 130° in the transition state ($^{Ph}$**1**-[**TS2**]) and up to 164° in the tridentate state of $^{Ph}$**L1** ($^{Ph}$**1**-[**I3**]).

**Reaction with the Third Alkyne Molecule.** From the metallacyclopentadiene complex, different mechanisms and intermediates have been proposed for the reaction of the third equivalent of alkyne (Scheme 1 and Introduction; see also Scheme S1 in the Supporting Information).[1h] Starting from Ni-MCP $^{Ph}$**1**-[**I3**], a [4 + 2] Diels−Alder type cycloaddition, which could proceed without the involvement of the nickel center, has been examined first (Figure 4, top; [4 + 2]). This

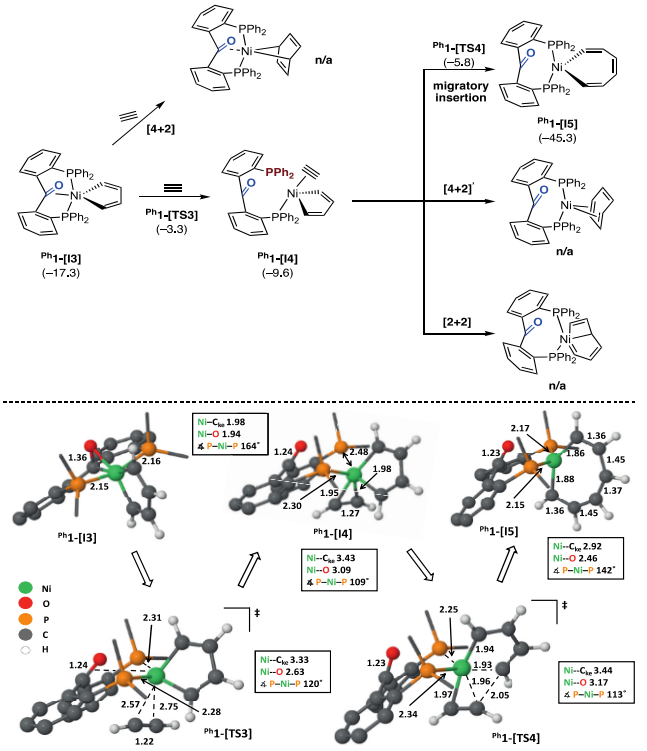


**Figure 4.** Reaction of acetylene with the nickelacyclopentadiene complex $^{Ph}$**1**-[**I3**] on the singlet spin state surface, with related Gibbs free energies given in kcal/mol (values in parentheses). (top) Schematic representation of the elementary steps, including the different evaluated pathways. (bottom) Optimized geometries (M06L-GD3/6-31g(d,p)) of intermediates and transition states. Hydrogen atoms (except from the alkyne and the hydrocarbyl ligands) and the phenyl substituents on the phosphorus arms have been omitted for clarity. Dotted lines in the transition states represent bonds being formed or broken. Bond lengths are given in Å.

pathway has been suggested to be favored for strong donor ligands or in reaction media containing strongly coordinating solvents.[14] The resulting 7-metallanorbornadienes[28] are frequently characterized as unstable species, which immediately decay to a benzene−metal $\pi$ adduct. Attempts to locate such a product from the [4 + 2] cycloaddition reaction of acetylene with $^{Ph}$**1**-[**I3**] were unsuccessful and resulted in either collapse of the structure to a $\eta^2$-benzene−nickel adduct ($^{Ph}$**1**-[**I7**]) or to the migratory insertion product ($^{Ph}$**1**-[**I5**] or $^{Ph}$**1**-[**I6**]). Similarly, an alternative intermolecular [4 + 2] cycloaddition generating an $\eta^4$-bound benzene−nickel complex (Figure 4, top; [4 + 2]′),[29] which can also been seen as a rearrangement product of the 7-nickellanorbornadiene compound, or a [2 + 2] cycloaddition mechanism (Figure 4, top; [2 + 2])[30] were also discarded, as no stationary points were


https://dx.doi.org/10.1021/acs.organomet.0c00172
Organometallics 2020, 39, 1998−2010

located along the energy profiles. The corresponding intermediates always rearranged into either a $\eta^2$-benzene nickel adduct ($^{Ph}$**1**-[**I7**]) or the migratory insertion product ($^{Ph}$**1**-[**I5**] or $^{Ph}$**1**-[**I6**]) during geometry optimization. Therefore, the reaction of the third acetylene molecule with the nickelacyclopentadiene complex $^{Ph}$**1**-[**I3**] is proposed to happen via migratory insertion (Figure 4, top; migratory insertion),[31] as also described in other dinuclear[10,21d] or mononuclear Ni systems.[7e,20,21c] The triplet-state analogue of $^{Ph}$**1**-[**I5**] is calculated to be less stable by 2.9 kcal/mol and 6.0 kcal/mol less stable than the pentacoordinate $^{Ph}$**1**-[**I6**] (section 2.3.1 and Figure S3 in the Supporting Information). However, it should be noted that the 2.9 kcal/mol difference between the singlet and triplet states is within the margin of error of the DFT method.

The formation of the nickelacyclopheptatriene intermediate $^{Ph}$**1**-[**I5**] from $^{Ph}$**1**-[**I3**] and acetylene occurs in a two-step process with initial $\eta^2$ coordination of the alkyne molecule to Ni to form the adduct $^{Ph}$**1**-[**I4**]. Such intermediates have been proposed for the construction of arenes from alkynes, on the basis of kinetic inhibition of the reaction of an isolated MCP with alkynes by donor ligands.[17c] Further evidence of the participation of a metallacyclopentadiene-alkyne species in the catalytic cycle was described by Vollhardt et al., who isolated a cobaltacyclopentadiene-monoalkyne intermediate in the intramolecular Co-catalyzed cyclotrimerization of bis(2-ethynylphenyl)ethyne.[24d,h] The Pörschke group also reported the synthesis of such species (Chart 1B; Introduction) in the reaction of a bimetallic Ni complex precursor supported by a 1,2-bis(diisopropylphosphino)ethane ligand with an excess of acetylene.[7a]

The association step of acetylene to $^{Ph}$**1**-[**I3**] is endergonic by +7.7 kcal/mol, and $^{Ph}$**1**-[**I4**] lies at −9.6 kcal/mol. A Gibbs free energy of activation ($\Delta G^{\circ,\ddagger}$) of +14.4 kcal/mol is associated with the coordination step. Upon binding of acetylene to Ni, the ketone decoordinates and the Ni−P bonds elongate to 2.30 Å (WBI(Ni−P) = 0.20) and 2.48 Å (WBI(Ni−P) = 0.18), the latter likely becoming a weak interaction. The geometry optimization of the transition state $^{Ph}$**1**-[**TS3**] reveals decoordination of the C═O unit ($C_{ke}$−O = 1.36 Å, Ni−$C_{ke}$ = 1.98 Å, and Ni−O = 1.94 Å in $^{Ph}$**1**-[**I3**] vs $C_{ke}$−O = 1.24 Å, Ni−$C_{ke}$ = 3.33 Å, and Ni−O = 2.63 Å in $^{Ph}$**1**-[**TS3**]) and elongation of the Ni−P bonds (from 2.15 and 2.16 Å in $^{Ph}$**1**-[**I3**] to 2.28 and 2.31 Å in $^{Ph}$**1**-[**TS3**], respectively). The significant decrease in the Ni−(C═O) $\pi$ interaction from the MCP $^{Ph}$**1**-[**I3**] intermediate is in accord with the WBIs from NBO analysis (WBI(Ni−$C_{ke}$) = 0.31 and WBI(Ni−O) = 0.23 in $^{Ph}$**1**-[**I3**] vs WBI(Ni−$C_{ke}$) = 0.06 and WBI(Ni−O) = 0.06 in $^{Ph}$**1**-[**TS3**]), while the weakening of the Ni−P bonds also correlates with their respective Wiberg bond indexes (WBIs(Ni−P) = 0.32 and 0.33 in $^{Ph}$**1**-[**I3**] vs 0.23 and 0.21 in $^{Ph}$**1**-[**TS3**]). $^{Ph}$**1**-[**TS3**] is characterized by a single imaginary frequency corresponding to the formation of a $\eta^2$-Ni−(C≡C) bond.

Next, the migratory insertion from $^{Ph}$**1**-[**I4**] to the metallacycloheptatriene $^{Ph}$**1**-[**I5**] ($G^\circ$ = −45.3 kcal/mol) via $^{Ph}$**1**-[**TS4**] ($G^\circ$ = −5.8 kcal/mol) is exergonic by −35.7 kcal/mol and requires a relatively small activation energy ($\Delta G^{\circ,\ddagger}$) of +3.8 kcal/mol. During this step, new Ni−vinyl and $\sigma$ C−C bonds are formed in a concerted fashion, while the carbonyl remains unbound. In addition, the Ni−P distances shorten again from 2.30 Å (WBI = 0.20) and 2.48 Å (WBI = 0.18) in $^{Ph}$**1**-[**I4**] to respectively 2.15 Å (WBI = 0.36) and 2.17 Å (WBI = 0.34) in $^{Ph}$**1**-[**I5**] via 2.34 Å (WBI = 0.22) and 2.25 Å (WBI = 0.25) in $^{Ph}$**1**-[**TS4**]. Similarly to the metallacyclopentadiene intermediate $^{Ph}$**1**-[**I3**], the calculated C−C bond lengths for $^{Ph}$**1**-[**I5**] (i.e., 1.45 Å for the C−C single bonds and ca. 1.36 Å for the C═C double bonds) are indicative of only slight $\pi$ delocalization within the metallacycle.

**Reductive Elimination of Benzene.** Finally, the last step in the catalytic cycle involves the reductive elimination of benzene and subsequent ligand exchange with acetylene (Figure 5). First, the reductive elimination of benzene from

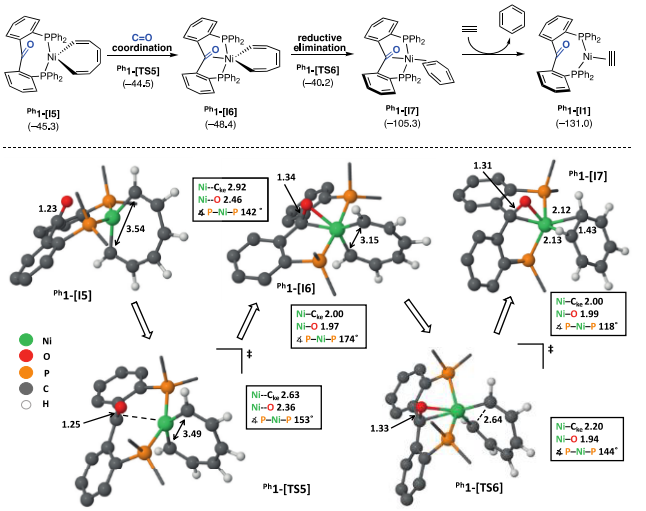


**Figure 5.** Reductive coupling and ligand exchange steps on the singlet spin state surface. (top) Schematic representation of the elementary steps, with related Gibbs free energies given in kcal/mol (values in parentheses). (bottom) Optimized geometries (M06L-GD3/6-31g-(d,p)) of the intermediates and the transition states during the reductive elimination step. Hydrogen atoms (except from the hydrocarbyl and benzene ligands) and the phenyl substituents on the phosphorus arms have been omitted for clarity. Dotted lines in the transition states represent bonds being formed. Bond lengths are given in Å.

the metallacycloheptatriene $^{Ph}$**1**-[**I5**] ($G^\circ$ = −45.3 kcal/mol) to form the Ni adduct $^{Ph}$**1**-[**I7**] ($G^\circ$ = −105.3 kcal/mol) appears to be assisted by a $\pi$ interaction of the central ketone with the Ni atom in intermediate $^{Ph}$**1**-[**I6**] ($G^\circ$ = −48.4 kcal/mol), which resembles the MCP intermediate $^{Ph}$**1**-[**I3**]. This concerted behavior is further borne out by a relaxed potential energy surface scan, in which all intermediates (i.e., $^{Ph}$**1**-[**I5**], $^{Ph}$**1**-[**I6**], and $^{Ph}$**1**-[**I7**]) and transition states (i.e., $^{Ph}$**1**-[**TS5**] and $^{Ph}$**1**-[**TS6**]) were located along the gradual shortening of the $C_\alpha$−$C_\alpha$ distance (section 2.3.1 and Figure S4 in the Supporting Information).

The C═O coordination step is very facile, with a $\Delta G^\circ$ value of −3.1 kcal/mol and an activation free energy $\Delta G^{\circ,\ddagger}$ of +0.8 kcal/mol. Subsequently, the reductive elimination process is exergonic by −56.9 kcal with a transition state, $^{Ph}$**1**-[**TS6**], located at +8.2 kcal/mol on the Gibbs free energy surface relative to $^{Ph}$**1**-[**I6**]. The accessibility of the 18-VE intermediates $^{Ph}$**1**-[**I6**] and $^{Ph}$**1**-[**I7**], in addition to the relatively low activation barrier associated with both the C═O coordination ($\Delta G^{\circ,\ddagger}$ = +0.8 kcal/mol) and reductive coupling ($\Delta G^{\circ,\ddagger}$ = +8.2 kcal/mol) steps, are likely to accelerate the reductive elimination step with respect to the coordination


https://dx.doi.org/10.1021/acs.organomet.0c00172
Organometallics 2020, 39, 1998−2010

of an additional alkyne to Ni. This binding mode is not available with the bidentate diphosphine ether Ni complex $^{Ph}$**3**, which could explain the difference in chemoselectivity between the two catalysts: namely, that more COT side products are detected with $^{Ph}$**3**, assuming that the formation of larger-size rings such as COT proceeds via a mechanism similar to that of the cyclotrimerization (i.e., alkyne association followed by migratory insertion).[16]

The calculated structure of $^{Ph}$**1**-[**I7**] resembles a previously characterized analogue bearing styrene as a coligand,[13] having both the ketone moiety and benzene molecule bound in a $\eta^2$ fashion. The relatively weak bond between nickel and benzene (Ni−C = 2.12 and 2.13 Å), associated with low WBIs of 0.17 and 0.18 (vs 0.41 and 0.42 for Ni−$C_{ac}$ in $^{Ph}$**1**-[**I1**]), allows the facile substrate substitution on $^{Ph}$**1**-[**I7**] in a subsequent step. Hence, the ligand exchange on $^{Ph}$**1**-[**I7**] between benzene and acetylene is spontaneous ($\Delta G°$ = −25.7 kcal/mol) and leads to the regeneration of the mono(acetylene) resting state $^{Ph}$**1**-[**I1**] for a new turnover, with the release of the cyclotrimerization product. $\pi$ complexes of arenes with different hapticities have been found in several reports along the reaction coordinate of metal-catalyzed cyclotrimerization reactions of alkynes.[1,14] An early example includes the isolation of an $\eta^6$-benzene−Ni(0) complex of a monoligated di(*tert*-butylphosphino)methane (dtbpm) ligand at −55 °C, from the cyclotrimerization of acetylene, providing more concrete evidence for the relevance of such structures to the catalytic cycle (see section 1.3 and Scheme S3 in the Supporting Information).[7d]

**Regioselectivity.** When the acetylene substrate is replaced by a substituted alkyne, the regioselectivity toward the production of the 1,2,4- or 1,3,5-trisubstituted cyclotrimerized benzene catalytic product is controlled by either the transition state between bis(alkyne) complex $^{Ph}$**1**-[**I2**] and metallacycle $^{Ph}$**1**-[**I3**] (step 2, oxidative coupling; $^{Ph}$**1**-[**TS2**]) or between $^{Ph}$**1**-[**I4**] and the migratory insertion compound $^{Ph}$**1**-[**I5**] (step 4, insertion; $^{Ph}$**1**-[**TS4**]). If the oxidative coupling transition state, i.e., $^{Ph}$**1**-[**TS2**], favors exclusively the formation of the 2,5- or 3,4-disubstituted metallacyclopentadiene, then $^{Ph}$**1**-[**TS4**] has no influence on the regioselectivity and the 1,2,4-substituted arene is selectively released at the end of the reaction (section 1.2 in the Supporting Information). Hence, using propyne as the model substrate, the arene regioselectivity control (1,2,4 vs 1,3,5) provided by the diphosphine ketone nickel system was addressed by transition state analysis of $^{Ph}$**1**-[**TS2**]-**Me** (Figure 6). The transition state connecting the bis(propyne) species ($^{Ph}$**1**-[**I2**]-**Me**) to the dimethylmetallacyclopentadiene intermediate ($^{Ph}$**1**-[**I3**]-**Me**) exhibits a preference for $^{Ph}$**1**-[**TS2**]-**2,5-Me** ($\Delta G^{\circ,\ddagger}$ = 15.7 kcal/mol), leading to the 2,5-dimethylnickelacyclopentadiene intermediate. The free energy barriers related to the generation of the 3,5-($\Delta G^{\circ,\ddagger}$ = 17.0 kcal/mol) and 2,4-dimethylnickelacyclopentadienes ($\Delta G^{\circ,\ddagger}$ = 18.4 kcal/mol) are relatively close to the values of $^{Ph}$**1**-[**TS2**]-**2,5-Me**. In contrast, for the 3,4-isomer a high $\Delta G^{\circ,\ddagger}$ value of 34.3 kcal/mol was found. The relatively high energy of $^{Ph}$**1**-[**TS2**]-**3,4-Me** also translates into structural dissimilarities with the other regioisomers. While $^{Ph}$**1**-[**TS2**]-**2,5-Me**, $^{Ph}$**1**-[**TS2**]-**3,5-Me**, and $^{Ph}$**1**-[**TS2**]-**2,4-Me** all resemble the unsubstituted metallacyclopentadiene $^{Ph}$**1**-[**TS2**], the steric bulk imposed by the methyl substituents of $^{Ph}$**1**-[**TS2**]-**3,4-Me** around the forming $\sigma$ C−C bond is reflected in an increased P−Ni−P angle (164° vs 130° in $^{Ph}$**1**-[**TS2**]) and longer C−C distance (2.91 Å vs 2.01 Å in $^{Ph}$**1**-[**TS2**]), as well as a

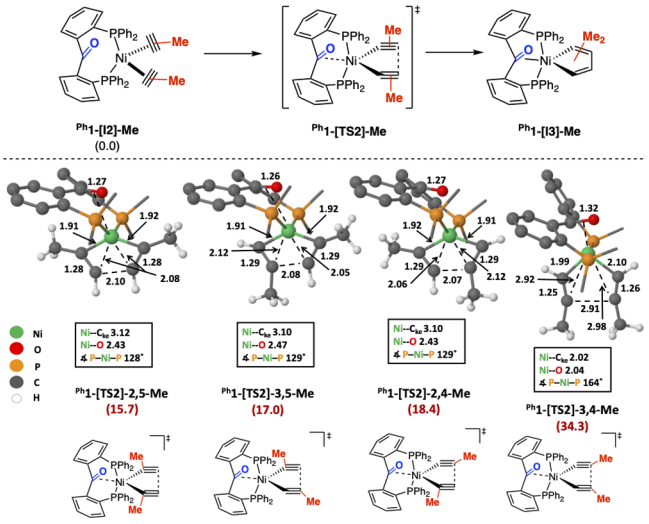


**Figure 6.** Oxidative coupling rate- and regio-selectivity-determining step on the singlet spin state surface, with propyne as the model substrate. (top) Schematic representation of the elementary step. (bottom) Optimized geometries (M06L-GD3/6-31g(d,p)) of the transition states. Hydrogen atoms (except from the alkyne and hydrocarbyl ligands) and the phenyl substituents on phosphorus arms have been omitted for clarity. The dotted lines in the transition states represent bonds being formed or broken. The bond lengths are given in Å. Values in parentheses are Gibbs free energies in kcal/mol.

decreased interaction between Ni and the alkynes (1.99−2.98 Å vs 1.91−2.08 Å in $^{Ph}$**1**-[**TS2**]). It negatively affects the Gibbs free energy of $^{Ph}$**1**-[**TS2**]-**3,4-Me**, which is not sufficiently compensated by an increased $\pi$ interaction with the central C═O unit (see also section 2.4 in the Supporting Information).

The calculated transition states are qualitatively consistent with the experimental observations. The small energy difference (1.3−2.7 kcal/mol) among $^{Ph}$**1**-[**TS2**]-**2,5-Me**, $^{Ph}$**1**-[**TS2**]-**3,5-Me**, and $^{Ph}$**1**-[**TS2**]-**2,4-Me** is in accord with the obtained mixture of 1,2,4- and 1,3,5-substituted arenes, with preference for the formation of the 1,2,4-substituted cyclotrimerization product. This selectivity pattern is more general for metal-catalyzed cyclotrimerization of terminal alkynes: the transition state in which the steric and electronic repulsion imposed by the substituents on the alkyne are minimal is commonly favored and is also closely related to the regioselectivity model proposed by Yamazaki.[17h]

**Comparison with the Tridentate Trisphosphine and the Bidentate Diphosphine Ether Ligands.** To shed more light on the differences among the ketone-based ligand $^{p\text{-}tol}$**1**, the pincer-type trisphosphine $^{p\text{-}tol}$**2**, and bidentate diphosphine ether $^{Ph}$**3** complexes in the Ni-catalyzed cyclotrimerization of terminal alkynes, these systems were also computationally explored for specific steps. The same DFT method as used in the previous section was used, with acetylene as the substrate and with model catalytic systems (i.e., phenyl substituents on phosphorus arms of the ligands, $^{Ph}$**L2** and $^{Ph}$**L3**, respectively; Chart 2A). For the ketone-based system, the intermediates and transition states are calculated on the singlet spin state surface and referenced to the mono(acetylene) resting states $^{Ph}$**2**-[**I1**] and $^{Ph}$**3**-[**I1**], respectively (Chart 2B).

*Tridentate Trisphosphine System.* First, the cyclotrimerization of acetylene into benzene was computationally investigated for the tris(phosphino) complex $^{Ph}$**2** (Figure 7; see also


https://dx.doi.org/10.1021/acs.organomet.0c00172
Organometallics 2020, 39, 1998−2010

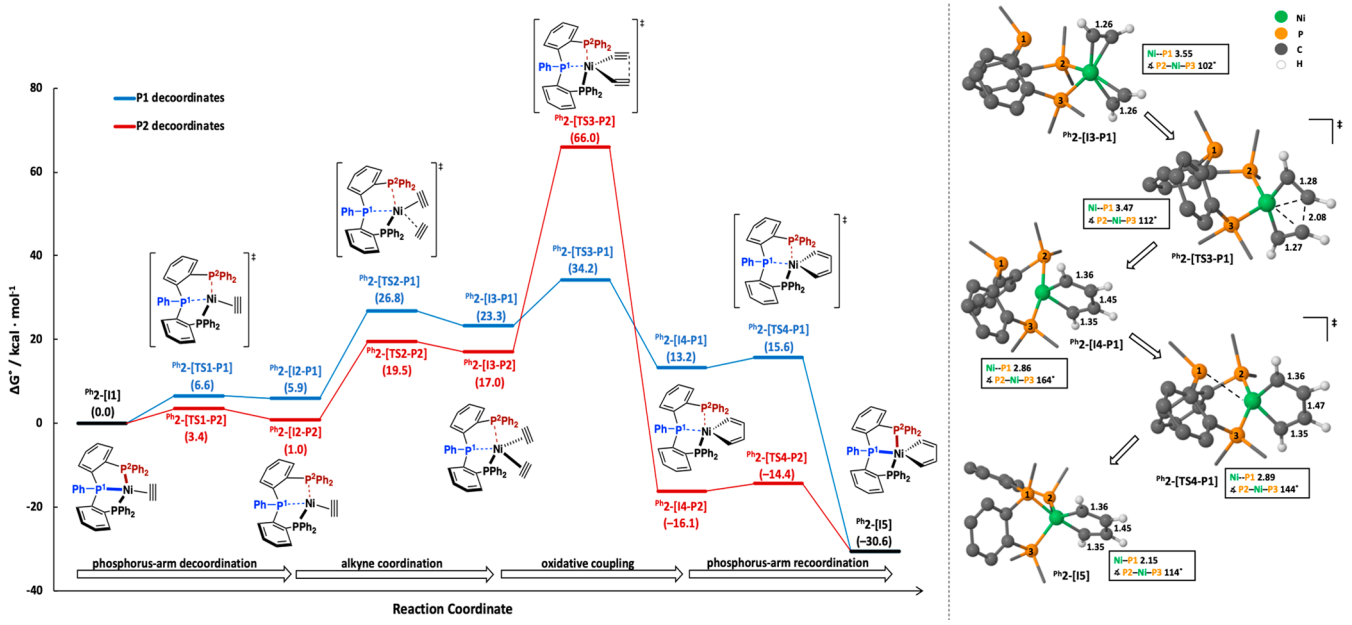


**Figure 7.** Formation of the nickelacyclopentadiene $^{Ph}$**2**-[**I5**] species, supported by a tridentate tris(phosphino) ligand ($^{Ph}$**L2**), as evaluated by DFT calculations. (left) Calculated relative Gibbs free energies (in kcal/mol; M06L-GD3/def2TZVP/SMD//M06L-GD3/6-31g(d,p), $T$ = 298.15 K) of the intermediates and transition states for the acetylene coordination and oxidative coupling steps, via two distinct pathways, starting from [($^{Ph}$**L2**)Ni(HC≡CH)] ($^{Ph}$**2**-[**I2**]), on the singlet spin state surface. For clarity, the free acetylene molecules are not shown but have been accounted for in the energy calculations. The values in parentheses are Gibbs free energies in kcal/mol. The dotted lines in the illustration of the transition states represent bonds being formed or broken. (right) Optimized geometries (M06L-GD3/6-31g(d,p)) of the intermediates and the transition state for the oxidative coupling step in the lower-energy pathway (blue lines from Gibbs free energy diagram). Hydrogen atoms (except from the alkyne and hydrocarbyl ligands) and the phenyl substituents on the phosphorus arms have been omitted for clarity. The dotted lines in the transition states represent bonds being formed or broken. The bond lengths are given in Å.

section 2.3.2 in the Supporting Information). The mono(acetylene) resting state $^{Ph}$**2**-[**I1**] is electronically saturated (18 VE), and decoordination of one phosphorus atom from the ligand is needed to enable the uptake of a second molecule of acetylene. Either the central phosphine, P1 (Figure 7, left; blue lines), or side phosphine, P2 (Figure 7, left; red lines) dissociates, both pathways leading to the formation of the pentacoordinate metallacyclopentadiene $^{Ph}$**2**-[**I5**], which is exergonic by −30.6 kcal/mol. Although the decoordination step of the side phosphine, P2, is more favorable ($\Delta G^\circ$ = 1.0 kcal/mol vs 5.9 kcal/mol for P1) with a lower activation barrier ($\Delta G^{\circ,\ddagger}$ = 3.4 kcal/mol vs 6.6 kcal/mol for P1), the calculated energy barrier of 49.0 kcal/mol (and 66.0 kcal/mol relative to $^{Ph}$**2**-[**I1**]) for the rate-determining oxidative coupling of the two acetylene fragments of the generated bis(acetylene) Ni species $^{Ph}$**2**-[**I3-P2**] to the metallacycle $^{Ph}$**2**-[**I4-P2**] is too high to be correlated with experimental observations. The high energy associated in the oxidative coupling step from $^{Ph}$**2**-[**I3-P2**] to $^{Ph}$**2**-[**I4-P2**] might suggest that a broader P−Ni−P bite angle is needed to facilitate the reaction and may partially explain the low catalytic performance of the *rac*-BINAP system in alkyne cyclotrimerization.[13]

For the bis(acetylene) complex, in which the central phosphine P1 is not bound to Ni ($^{Ph}$**2**-[**I3-P1**]), only 10.9 kcal/mol is required to overcome the activation barrier of the oxidative coupling step (vs 15.8 kcal/mol for the $^{Ph}$**L1**-based system). However, because of the preceding endergonic alkyne coordination step, the overall activation Gibbs free energy (34.2 kcal/mol) is significantly higher. This large activation barrier can explain the generally low activity of the trisphosphine-based catalyst $^{p\text{-tol}}$**2** in alkyne cyclotrimerization reactions. The stronger binding character of the phosphine ligand in comparison to the ketone moiety stabilizes the formed pentacoordinate nickelacycle to a greater extent (i.e., $G^\circ$($^{Ph}$**2**-[**I5**]) = −30.6 kcal/mol vs $G^\circ$($^{Ph}$**1**-[**I3**]) = −17.3 kcal/mol, relative to the mono(alkyne) nickel complex). In contrast to $^{Ph}$**1**-[**I3**], the formation of the pentacoordinate nickelacycle $^{Ph}$**2**-[**I5**] happens in a stepwise fashion, with first the oxidative coupling ($^{Ph}$**2**-[**I3-P1**] → $^{Ph}$**2**-[**I4-P1**]; $\Delta G^\circ$= −9.1 kcal/mol, $\Delta G^{\circ,\ddagger}$ = +10.9 kcal/mol), and consecutive facile recoordination of the central P atom($^{Ph}$**2**-[**I4−P1**] → $^{Ph}$**2**-[**I5**]; $\Delta G^\circ$= −43.8 kcal/mol, $\Delta G^{\circ,\ddagger}$ = +2.4 kcal/mol). The stepwise reactivity might be responsible for structural differences in the geometry from the oxidative coupling transition state ($^{Ph}$**2**-[**TS3-P1**]), in comparison to the related diphosphine ketone transition state ($^{Ph}$**1**-[**TS2**]), with a P−Ni−P angle of 112° versus 130° for $^{Ph}$**1**-[**TS2**]. This might influence the regioselectivity of the process with substituted alkynes (i.e., ratio between 1,2,4- and 1,3,5-trisubstituted arene products).

*Bidentate Diphosphine Ether Ligand.* With regard to the diphosphine ether ($^{Ph}$**L3**) Ni system, the DFT comparison until the formation of the key nickellacyclopentadiene species $^{Ph}$**3**-[**I3**] (Figure 8) is consistent with the lower catalytic performances of $^{Ph}$**3** in alkyne cyclotrimerization reactions in comparison to the diphosphine ketone based catalyst $^{p\text{-tol}}$**1**. For the acetylene association ($^{Ph}$**3**-[**I1**] → $^{Ph}$**3**-[**I2**]), both the energies, $\Delta G^\circ$= 11.6 kcal/mol (vs 10.4 kcal/mol for $^{Ph}$**1**-[**I1**]) and $\Delta G^{\circ,\ddagger}$ = 12.2 kcal/mol (vs 13.9 kcal/mol for $^{Ph}$**1**-[**I1**]) and the geometries (from a tricoordinated 16-VE mono(acetylene) to a tetracoordinate 18-VE bis(acetylene) compound) are similar to those calculated with the $^{Ph}$**L1** analogue. However, the rate-determining oxidative coupling step ($^{Ph}$**3**-[**I2**] → $^{Ph}$**3**-[**I3**]) differs significantly. The transition state, $^{Ph}$**3**-[**TS2**], lies


https://dx.doi.org/10.1021/acs.organomet.0c00172
Organometallics 2020, 39, 1998−2010

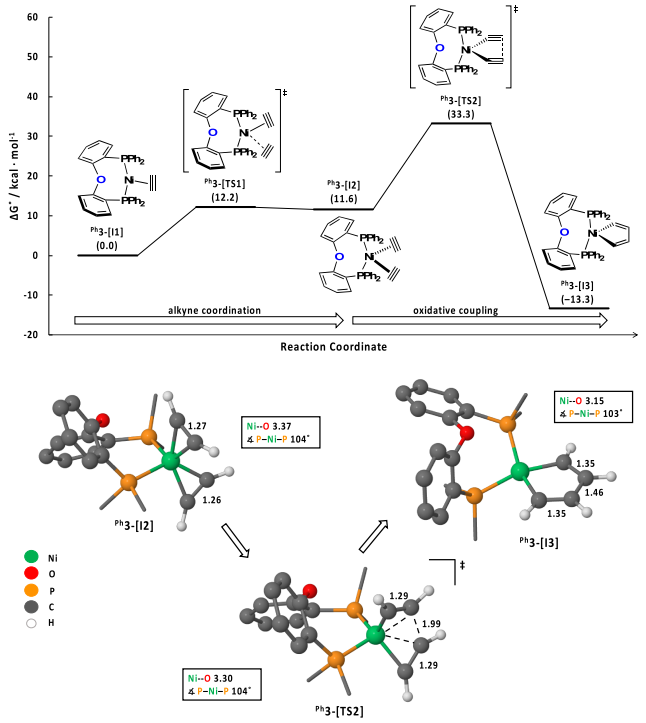


**Figure 8.** Formation of the nickelacyclopentadiene $^{Ph}$**3**-[**I3**] species, supported by a bidentate bis(phosphino) ether ligand ($^{Ph}$**L3**), as evaluated by DFT calculations. (top) Calculated relative Gibbs free energies (in kcal/mol; M06L-GD3/def2TZVP/SMD//M06L-GD3/6-31g(d,p), $T$ = 298.15 K) for the acetylene coordination and the oxidative coupling steps in the cyclotrimerization of acetylene into benzene, starting from [($^{Ph}$**L3**)Ni(HC≡CH)] ($^{Ph}$**3**-[**I1**]), on the singlet spin state surface. For clarity, the free acetylene molecules are not shown but have been accounted for in energy calculations. The values in parentheses are Gibbs free energies in kcal/mol. The dotted lines in the illustration of the transition states represent bonds being formed. (bottom) Optimized geometries (M06L-GD3/6-31g(d,p)) of the intermediates and the transition state for the oxidative coupling step. Hydrogen atoms (except for the alkyne and hydrocarbyl ligands) and the phenyl substituents on the phosphorus arms have been omitted for clarity. The dotted lines in $^{Ph}$**3**-[**TS2**] represent bonds being formed or broken. The bond lengths are given in Å.

at 33.3 kcal/mol on the energy surface, 7.1 kcal/mol higher than $^{Ph}$**1**-[**TS2**], with an activation energy barrier, $\Delta G^{\circ,\ddagger}$, of 21.7 kcal/mol, 5.9 kcal/mol greater than the 15.8 kcal/mol needed for the ketone system. During this oxidative coupling step, no significant modifications in the geometry of $^{Ph}$**L3** around the metal center are observed, with a constant P–Ni–P bite angle (from 104° in $^{Ph}$**3**-[**I2**], via 104° in $^{Ph}$**3**-[**TS2**], to 103° in $^{Ph}$**3**-[**I3**]) and without any significant Ni–O coordination. These results support the idea that the adaptive behavior of the central ketone moiety of the ligand $^{Ph}$**L1** during the oxidative coupling elementary step contributes to the overall reduction of the activation energy barrier of the reaction: first by stabilizing the metallacyclopentadiene key intermediate and second by stabilizing the transition state through additional (partial) $\pi$ interaction of C=O with Ni.

## CONCLUSIONS

The computational study presented above, together with experimental observations,[13] supports the catalytic cycle depicted in Scheme 2 for the cyclotrimerization of terminal alkynes catalyzed by nickel complexes of a bis(phosphino)-benzophenone ligand ($^{Ph}$**L1**). Key aspects are highlighted here.

First, the resting state of the catalyst is a mono(alkyne) complex in which the ligand $^{Ph}$**L1** is bound to the metal center in a $\kappa^2$(P,P) mode. This makes the uptake of the second alkyne equivalent easier than with the triphosphine ligand $^{Ph}$**L2** system, lowering the overall energy barrier, which accounts for the difference in activity between these two systems.

Next, the key metallacycle intermediate derived from $^{Ph}$**L1** is stabilized by an additional $\eta^2$ coordination of the C=O $\pi$-acceptor unit. This reduces the associated energy barrier by 5.9 kcal/mol with respect to the bidentate ligand $^{Ph}$**L3**, explaining the higher activity observed with $^{Ph}$**L1**. Furthermore, the comparison of isomeric transition states derived from propyne reveals the favored generation of the 2,5-substituted MCP species, in agreement with the major production of the 1,2,4-trisubstituted arene isomer observed experimentally.

Subsequently, the labile Ni–(C=O) bond enables the stepwise coordination and migratory insertion of the third equivalent of alkyne into the MCP to form a metal-lacycloheptatriene intermediate (steps 4 and 5). This migratory insertion pathway differs from that calculated with the triphosphine ligand $^{Ph}$**L2**, for which the strong central P–Ni bond only permits an energetically demanding, stepwise [4 + 2] cycloaddition pathway (section 2.3.2 in the Supporting Information).

Finally, reductive coupling of the substituted arene product (steps 6 and 7) is assisted through the $\pi$ recoordination of the ketone moiety to Ni (step 6), favoring the formation of a nickel– benzene adduct (step 7) and possibly preventing the coordination of a fourth molecule of alkyne, which is likely the first step toward cyclotetrameric side products. This accounts for the higher selectivity of $^{Ph}$**L1** for trimers versus tetramers in comparison to the bidentate $^{Ph}$**L3**.

All in all, the results presented in this study highlight the specific advantages of a chelating $\pi$-acceptor ligand in nickel catalysis. The uncovered metal–ligand cooperative mechanism, in which the $\pi$-coordinating moiety adapts its binding to the requirements of specific reactive intermediates or transition states, is likely to be of importance for other catalytic transformations. Accordingly, it can be envisioned that nickel complexes of tethered $\pi$-acceptor ligands will find other applications in catalytic processes, which is the subject of further investigations in our laboratories.

## EXPERIMENTAL SECTION

**Computational Methods.** DFT (density functional theory) results were obtained using the Gaussian 16 software package.[32] Restricted (R) and unrestricted (U) geometry optimizations used the M06L (Minnesota 2006, local) functional[33] and the 6-31g(d,p) basis set on all atoms. The structures were optimized with added empirical dispersion (GD3)[34] and without any symmetry restraints and are either minima or transition states, as checked by the presence of 0 or 1 imaginary frequency, respectively. Frequency analyses were performed on all calculations at a M06L-GD3/6-31g(d,p) level of theory, and thermochemical calculations for Gibbs free energies were performed at a temperature of 298.15 K and a default pressure of 1 atm. Single-point (SP) calculations were performed on the optimized geometries at the M06L/def2TZVP level of theory with the SMD (solvation based on density) toluene solvent model and added empirical dispersion (GD3). The Gibbs free energies of formation of the reactants, products, and transition states were calculated from the optimized structures by SP calculations and by adding the thermal correction to the Gibbs free energy. The transition state analysis was performed using either the QST3 (synchronous transit-guided quasi


https://dx.doi.org/10.1021/acs.organomet.0c00172
Organometallics 2020, 39, 1998–2010

**Scheme 2. Proposed Catalytic Cycle for the Cyclotrimerization of Terminal Alkynes Catalyzed by [($^{Ph}$L1)Ni(BPI)] ($^{Ph}$1) or by *in Situ* Generation of the Active Intermediate with $^{Ph}$L1 + Ni(cod)$_2$, as Evaluated by DFT Calculations**[a]

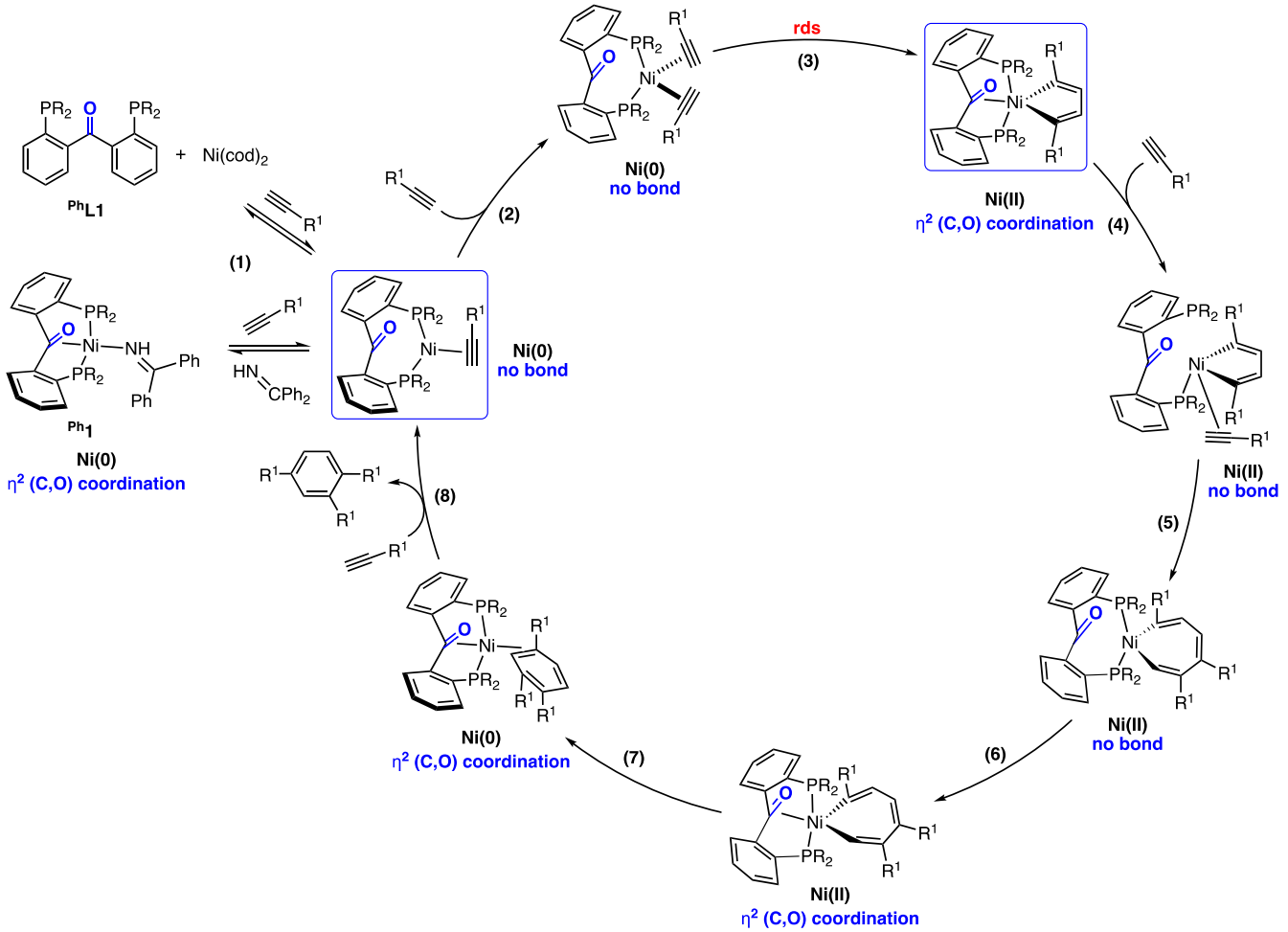


[a]Framed compounds are proposed key intermediates for activity and selectivity. Abbreviations: rds = rate-determining step. R = Ph. Legend: (1) substrate exchange; (2) alkyne association; (3) oxidative coupling; (4) alkyne association; (5) migratory insertion; (6) C═O coordination; (7) reductive elimination; (8) substrate exchange and release of the 1,2,4-trisubstituted cyclotrimerized product.

Newton number 3; opt = qst3, calcfc, noeigentest) method or the transition state optimization (opt = ts, calcfc, noeigentest) using a transition state guess that was located by a rigid potential energy surface (PES) scan (opt = modredundant) on selected bond or angle axis coordinates, connecting the reactant and the product. The transition state was validated either by an intrinsic reaction coordinate (IRC) scan along the imaginary vibrational frequency or by the geometry optimization of the TS toward the reactant and product. For NBO (natural bond orbital) calculations, the NBO6 program,[35] up to the NLMO (natural localized molecular orbital) basis set, was used at the M06L/def2TZVP level of theory from the optimized geometries. The pictures derived from the DFT calculations have been generated using the Jmol software.[36] The ligand exchange reaction of the benzophenone imine ligand (BPI) in the precatalyst [($^{p\text{-tol}}$L1)Ni(BPI)] ($^{p\text{-tol}}$1) for the diphenylacetylene coligand (Ph−C≡C−Ph) was used as a model to evaluate the accuracy of the computational method: i.e., $^{p\text{-tol}}$1 + Ph−C≡C−Ph ⇄ [($^{p\text{-tol}}$L1)Ni-(Ph−C≡C−Ph)] + BPI (section 2.2 in the Supporting Information). M06L-GD3/def2TZVP//M06L-GD3/6-31g(d,p) calculation at $T$ = 298.15 K with the SMD model predicts a $\Delta G°$ value of 2.7 kcal/mol, which correlates closely to the experimental value of 3.1 kcal/mol[13] measured by $^1$H NMR.

## ■ ASSOCIATED CONTENT

### Supporting Information

The Supporting Information is available free of charge on the ACS Publications Web site. (PDF) (XYZ) The Supporting Information is available free of charge at https://pubs.acs.org/doi/10.1021/acs.organomet.0c00172.

DFT details and additional discussions (PDF)

Cartesian coordinates of DFT optimized structures (XYZ)

## ■ AUTHOR INFORMATION


### Corresponding Author

**Marc-Etienne Moret** − *Utrecht University, Organic Chemistry and Catalysis, Debye Institute for Nanomaterials Science, Faculty of Science, 3584 CG Utrecht, The Netherlands;* orcid.org/0000-0002-3137-6073; Email: m.moret@uu.nl

### Author

**Alessio F. Orsino** − *Utrecht University, Organic Chemistry and Catalysis, Debye Institute for Nanomaterials Science, Faculty of Science, 3584 CG Utrecht, The Netherlands*

Complete contact information is available at:




https://dx.doi.org/10.1021/acs.organomet.0c00172
*Organometallics* 2020, 39, 1998−2010

https://pubs.acs.org/10.1021/acs.organomet.0c00172

### Notes

The authors declare no competing financial interest.

## ■ ACKNOWLEDGMENTS

We acknowledge funding from the NWO council under grant agreement ECHO-STIP, project no. 717.014.009. This work was sponsored by the NWO Exacte en Natuurwetenschappen (Physical Sciences) for the use of supercomputer facilities, with financial support from the Nederlandse Organisatie voor Wetenschappelijk Onderzoek (Netherlands Organization for Scientific Research, NWO). The DFT work was carried out on the Dutch national e-infrastructure with the support of the SURF Foundation.

## ■ REFERENCES

(1) For reviews and books on metal-catalyzed alkyne cyclotrimerization reactions, see: (a) Saito, S.; Yamamoto, Y. Recent Advances in the Transition-Metal-Catalyzed Regioselective Approaches to Polysubstituted Benzene Derivatives. *Chem. Rev.* **2000**, *100*, 2901−2915. (b) Chopade, P. R.; Louie, J. [2 + 2+2] Cycloaddition Reactions Catalyzed by Transition Metal Complexes. *Adv. Synth. Catal.* **2006**, *348*, 2307−2327. (c) Shibata, T.; Tsuchikama, K. Recent Advances in Enantioselective [2 + 2+2] Cycloaddition. *Org. Biomol. Chem.* **2008**, *6*, 1317−1323. (d) Galan, B. R.; Rovis, T. Beyond Reppe: Building Substituted Arenes by [2 + 2+2] Cycloadditions of Alkynes. *Angew. Chem., Int. Ed.* **2009**, *48*, 2830−2834. (e) Domínguez, G.; Pérez-Castells, J. Recent Advances in [2 + 2+2] Cycloaddition Reactions. *Chem. Soc. Rev.* **2011**, *40*, 3430−3444. (f) Broere, D.; Ruijter, E. Recent Advances in Transition-Metal-Catalyzed [2 + 2+2]-Cyclo(Co)Trimerization Reactions. *Synthesis* **2012**, *44*, 2639−2672. (g) Domínguez, G.; Pérez-Castells, J. Alkenes in [2 + 2+2] Cycloadditions. *Chem. - Eur. J.* **2016**, *22*, 6720−6739. (h) Yamamoto, K.; Nagae, H.; Tsurugi, H.; Mashima, K. Mechanistic Understanding of Alkyne Cyclotrimerization on Mononuclear and Dinuclear Scaffolds: [4 + 2] Cycloaddition of the Third Alkyne onto Metallacyclopentadienes and Dimetallacyclopentadienes. *Dalton Trans.* **2016**, *45*, 17072−17081. (i) Schore, N. E. Transition Metal-Mediated Cycloaddition Reactions of Alkynes in Organic Synthesis. *Chem. Rev.* **1988**, *88*, 1081−1119. (k) *Modern Alkyne Chemistry: Catalytic and Atom-Economic Transformations*; Trost, B. M., Li, C.-J., Eds.; Wiley-VCH: Weinheim, Germany, 2015.

(2) For examples of alkyne cyclotrimerization for the synthesis of natural products, see: (a) Aalbersberg, W. G. L.; Barkovich, A. J.; Funk, R. L.; Hillard, R. L.; Vollhardt, K. P. C. Transition Metal Catalyzed Acetylene Cyclizations. 4,5-Bis(Trimethylsilyl)-Benzocyclobutene, a Highly Strained, Versatile Synthetic Intermediate. *J. Am. Chem. Soc.* **1975**, *97*, 5600−5602. (b) Vollhardt, K. P. C. Transition-Metal-Catalyzed Acetylene Cyclizations in Organic Synthesis. *Acc. Chem. Res.* **1977**, *10*, 1−8. (c) Vollhardt, K. P. C. Cobalt-Vermittelte [2 + 2+2]-Cycloadditionen: Eine Ausgereifte Synthesestrategie. *Angew. Chem.* **1984**, *96*, 525−541.

(3) Reppe, W.; Schlichting, O.; Klager, K.; Toepel, T. Cyclisierende Polymerisation von Acetylen I Über Cyclooctatetraen. *Justus Liebigs Ann. Chem.* **1948**, *560*, 1−92.

(4) Reppe, W.; Schweckendiek, W. J. Cyclisierende Polymerisation von Acetylen. III Benzol, Benzolderivate Und Hydroaromatische Verbindungen. *Justus Liebigs Ann. Chem.* **1948**, *560*, 104−116.

(5) For an extensive list of examples of nickel-catalyzed cyclotrimerization of alkynes, see ref 13 and references cited therein.

(6) (a) Eisch, J. J.; Damasevitz, G. A. Stereospecific Alkylation of Alkynes by Bis(π-Allyl)Nickel and the Mechanism of Oligomerization of Alkynes by Nickel(0). *J. Organomet. Chem.* **1975**, *96*, C19−C22. (b) Eisch, J. J.; Galle, J. E. The Role of Nickelole Intermediates in the Oligomerization of Alkynes. *J. Organomet. Chem.* **1975**, *96*, C23−C26. (c) Eisch, J. J.; Galle, J. E.; Aradi, A. A.; Bolesawski, M. P. Organic Chemistry of Subvalent Transition Metal Complexes. *J. Organomet. Chem.* **1986**, *312* (3), 399−416.

(7) (a) Pörschke, K.-R. Coupling of Two Ethyne Molecules at a Nickel Center to Form a Nickelacyclopentadiene Complex. *Angew. Chem., Int. Ed. Engl.* **1987**, *26*, 1288−1290. (b) Bonrath, W.; Michaelis, S.; Pörschke, K.-R.; Gabor, B.; Mynott, R.; Krüger, C. Reaktion von (1,4-Diazabutadien)Bis(Alken)Nickel(0)-Komplexen Mit Ethin. *J. Organomet. Chem.* **1990**, *397*, 255−260. (c) Michaelis, S.; Pörschke, K.-R.; Krüger, C.; Mynott, R.; Goddard, R. Struktur Und Dynamik von $[(2,6\text{-}Me_2Ph\text{-}Dad)Ni]_2((^2(1,4),(^4(1-4)\text{-}C_4H_4\}$. *J. Organomet. Chem.* **1992**, *426*, 130−141. (d) Nickel, T.; Goddard, R.; Krüger, C.; Pörschke, K.-R. Cyclotrimerization of Ethyne on the Complex Fragment $[(r^1\text{-}tBu_2PCH_2PtBu_2)Ni^0]$ with Formation of an $]^6$-Benzene-Nickel(0) Complex. *Angew. Chem., Int. Ed. Engl.* **1994**, *33*, 879−882. (e) Max-Planck-Institut Für Kohlenforschung Mülheim an Der Ruhr. In *Max-Planck-Gesellschaft Jahrbuch 1998 (Max Planck Society Yearbook 1998)*; Deutschmann, S., Ed.; Verlag Vandenhoeck & Ruprecht: Göttingen, Germany, 1999; pp 521−527.

(8) Rodrigo, S. K.; Powell, I. V.; Coleman, M. G.; Krause, J. A.; Guan, H. Efficient and Regioselective Nickel-Catalyzed [2 + 2+2] Cyclotrimerization of Ynoates and Related Alkynes. *Org. Biomol. Chem.* **2013**, *11*, 7653−7657.

(9) Pal, S.; Uyeda, C. Evaluating the Effect of Catalyst Nuclearity in Ni-Catalyzed Alkyne Cyclotrimerizations. *J. Am. Chem. Soc.* **2015**, *137*, 8042−8045.

(10) Hollingsworth, R. L.; Bheemaraju, A.; Lenca, N.; Lord, R. L.; Groysman, S. Divergent Reactivity of a New Dinuclear Xanthene-Bridged Bis(Iminopyridine) Di-Nickel Complex with Alkynes. *Dalton Trans.* **2017**, *46*, 5605−5616.

(11) Verhoeven, D. G. A.; Moret, M.-E. Metal-Ligand Cooperation at Tethered π-Ligands. *Dalton Trans.* **2016**, *45*, 15762−15778.

(12) For the first report describing the synthesis of $^{Ph}$**L1**, see: Mikami, K.; Wakabayashi, K.; Aikawa, K. Achiral" Benzophenone Ligand for Highly Enantioselective Ru Catalysts in Ketone Hydrogenation. *Org. Lett.* **2006**, *8*, 1517−1519.

(13) Orsino, A. F.; Gutiérrez del Campo, M.; Lutz, M.; Moret, M.-E. Enhanced Catalytic Activity of Nickel Complexes of an Adaptive Diphosphine-Benzophenone Ligand in Alkyne Cyclotrimerization. *ACS Catal.* **2019**, *9*, 2458−2481.

(14) For reviews on mechanistic studies in metal-catalyzed cyclotrimerization reactions, see ref 1h and: Varela, J. A.; Saá, C. CpRuCl- and CpCo-Catalyzed or Mediated Cyclotrimerizations of Alkynes and [2 + 2+2] Cycloadditions of Alkynes to Alkenes: A Comparative DFT Study. *J. Organomet. Chem.* **2009**, *694*, 143−149.

(15) For a review on metallacyclopentadienes, see: Ma, W.; Yu, C.; Chen, T.; Xu, L.; Zhang, W.-X.; Xi, Z. Metallacyclopentadienes: Synthesis, Structure and Reactivity. *Chem. Soc. Rev.* **2017**, *46*, 1160−1192.

(16) Wang, C.; Xi, Z. Metal Mediated Synthesis of Substituted Cyclooctatetraenes. *Chem. Commun.* **2007**, *48*, 5119−5133.

(17) For examples of mechanistic studies on CpCo-type-catalyzed alkyne cyclotrimerization, see ref 14 and: (a) Hardesty, J. H.; Koerner, J. B.; Albright, T. A.; Lee, G. Y. Theoretical Study of the Acetylene Trimerization with CpCo. *J. Am. Chem. Soc.* **1999**, *121*, 6055−6067. (b) Dahy, A. R. A.; Koga, N. Theoretical Study on the Transformation of Bis(acetylene)cobalt to Cobaltacyclopentadiene and the Regioselectivity in this Transformation. *Bull. Chem. Soc. Jpn.* **2005**, *78*, 781−791. (c) McAlister, D. R.; Bercaw, J. E.; Bergman, R. G. Parallel Reaction Pathways in the Cobalt-Catalyzed Cyclotrimerization of Acetylenes. *J. Am. Chem. Soc.* **1977**, *99*, 1666−1668. (d) Agenet, N.; Gandon, V.; Vollhardt, K. P. C.; Malacria, M.; Aubert, C. Cobalt-Catalyzed Cyclotrimerization of Alkynes: The Answer to the Puzzle of Parallel Reaction Pathways. *J. Am. Chem. Soc.* **2007**, *129*, 8860−8871. (e) Yamazaki, H.; Hagihara, N. New Phenylacetylene Complexes of Cobalt. *J. Organomet. Chem.* **1967**, *7*, P22−P23. (f) Wakatsuki, Y.; Kuramitsu, T.; Yamazaki, H. Cobaltacyclopentadiene Complexes as Starting Materials in the Synthesis of Substituted Benzenes, Cyclohexadienes, Thiophenes, Selenophenes and Pyrroles. *Tetrahedron Lett.* **1974**, *15*, 4549−4552. (g) Lee, G.; Koerner, J. B.; Albright,

T. A. The Mechanism for Cyclooligomerization of Acetylene: The Structures of $CpCo(C_4H_4)$ and $CpCo(\eta^2\text{-}C_2H_2)_2$ as Intermediates. *Bull. Korean Chem. Soc.* **1993**, *14*, 320−322. (h) Wakatsuki, Y.; Nomura, O.; Yamazaki, H.; Kitaura, K.; Morokuma, K. Cobalt Metallacycles. 11. On the Transformation of Bis(Acetylene)Cobalt to Cobaltacyclopentadiene. *J. Am. Chem. Soc.* **1983**, *105*, 1907−1912.

(18) For examples of mechanistic studies on CpRu-type-catalyzed alkyne cyclotrimerization, see refs 1h and 11 and: (a) Kirchner, K.; Calhorda, M. J.; Schmid, R.; Veiros, L. F. Mechanism for the Cyclotrimerization of Alkynes and Related Reactions Catalyzed by CpRuCl. *J. Am. Chem. Soc.* **2003**, *125*, 11721−11729. (b) Calhorda, M. J.; Costa, P. J.; Kirchner, K. A. Benzene and Heterocyclic Rings Formation in Cycloaddition Reactions Catalyzed by RuCp Derivatives: DFT studies. *Inorg. Chim. Acta* **2011**, *374*, 24−35. (c) Rüba, E.; Schmid, R.; Kirchner, K.; Calhorda, M. J. Ruthenium-Mediated Cyclotrimerization of Alkynes Utilizing the Cationic Complex $[RuCp(CH_3CN)_3]PF_6$. *J. Organomet. Chem.* **2003**, *682*, 204−211. (d) Becker, E.; Mereiter, K.; Puchberger, M.; Schmid, R.; Kirchner, K.; Doppiu, A.; Salzer, A. Novel [2 + 2+1] Cyclotrimerization of Alkynes Mediated by Bidentate Cyclopentadienyl-Phosphine Ruthenium Complexes. *Organometallics* **2003**, *22*, 3164−3170. (e) Yamamoto, Y.; Arakawa, T.; Ogawa, R.; Itoh, K. Ruthenium(II)-Catalyzed Selective Intramolecular [2 + 2+2] Alkyne Cyclotrimerizations. *J. Am. Chem. Soc.* **2003**, *125*, 12143−12160.

(19) For examples of mechanistic studies on Rh-catalyzed alkyne cyclotrimerization, see: (a) Orian, L.; Swart, M.; Bickelhaupt, F. M. Indenyl Effect due to Metal Slippage? Computational Exploration of Rhodium-Catalyzed Acetylene [2 + 2+2] Cyclotrimerization. *ChemPhysChem* **2014**, *15*, 219−228. (b) Dachs, A.; Osuna, S.; Roglans, A.; Solà, M. Density Functional Study of the [2 + 2+2] Cyclotrimerization of Acetylene Catalyzed by Wilkinson's Catalyst, $RhCl(PPh_3)_3$. *Organometallics* **2010**, *29*, 562−569. (c) Orian, L.; Van Stralen, J. N. P.; Bickelhaupt, F. M. Cyclotrimerization Reactions Catalyzed by Rhodium(I) Half-Sandwich Complexes: A Mechanistic Density Functional Study. *Organometallics* **2007**, *26*, 3816−3830. (d) Collman, J. P.; Kang, J. W.; Little, W. F.; Sullivan, M. F. Metallocyclopentadiene Complexes of Iridium and Rhodium and Their Role in the Catalytic Cyclotrimerization of Disubstituted Acetylenes. *Inorg. Chem.* **1968**, *7*, 1298−1303.

(20) For a DFT mechanistic study on Ni-catalyzed cyclotetramerization of acetylene using Reppe's catalyst, see: Straub, B. F.; Gollub, C. Mechanism of Reppe's Nickel-Catalyzed Ethyne Tetramerization to Cyclooctatetraene: A DFT Study. *Chem. - Eur. J.* **2004**, *10*, 3081−3090.

(21) For mechanistic studies on Ni-catalyzed cyclotrimerization of alkynes from other groups than ours, see refs 6, 7, 9, and 10 and: (a) Pasynkiewicz, S.; Pietrzykowski, A.; Kryza-Niemiec, B.; Zachara, J. The First Structurally Characterized Trinickel Cluster with an Open Structure: Crystal and Molecular Structure of $CpNi[\mu\text{-}\eta^4\text{-}PhC = C(Ph)\text{-}C(Ph)=CPh]Ni(\mu\text{-}\eta^2\eta^2\text{-}PhC\text{-}CPh)NiCp$. *J. Organomet. Chem.* **1998**, *566*, 217−224. (b) Colbran, S. B.; Robinson, B. H.; Simpson, J. Synthesis, Structure, and Redox Properties of $[(\eta\text{-}C_5H_5)Fe\{\}\text{-}\sigma{:}\eta^4\text{-}NiC_4R_4(\eta\text{-}C_5H_5)\}]$. A Ferrocene Analogue with a Nickelapentadiene Ring. *Organometallics* **1985**, *4*, 1594−1601. (c) Müller, C.; Lachicotte, R. J.; Jones, W. D. Catalytic C-C Bond Activation in Biphenylene and Cyclotrimerization of Alkynes: Increased Reactivity of P, N- versus P, P-Substituted Nickel Complexes. *Organometallics* **2002**, *21*, 1975−1981. (d) Kwon, D.-H.; Proctor, M.; Mendoza, S.; Uyeda, C.; Ess, D. H. Catalytic Dinuclear Nickel Spin Crossover Mechanism and Selectivity for Alkyne Cyclotrimerization. *ACS Catal.* **2017**, *7*, 4796−4804.

(22) In *NIST Chemistry WebBook, NIST Standard Reference Database Number 69*; Linstrom, P. J., Mallard, W. G., Eds.; National Institute of Standards and Technology: Gaithersburg, MD, 2018; DOI: 10.18434/T4D303 (accessed March 9, 2020).

(23) (a) Hopmann, K. H. How To Make Your Computational Paper Interesting and Have It Published. *Organometallics* **2019**, *38*, 603−605. (b) Ryu, H.; Park, J.; Kim, H. K.; Park, J. Y.; Kim, S. T.; Baik, M. H. Pitfalls in Computational Modeling of Chemical Reactions and How to Avoid Them. *Organometallics* **2018**, *37*, 3228−3239.

(24) For examples of metallacyclopentadienes, see refs 6, 7a−c, 9, 12, and 17c,e,f and: (a) Yamazaki, H.; Wakatsuki, Y. Cobalt Metallocycles. XIII. Preparation and x-Ray Crystallography of Cobaltacyclopentadiene and Dinuclear Cobalt Complexes. *J. Organomet. Chem.* **1984**, *272*, 251−263. (b) Strickler, J. R.; Wexler, P. A.; Wigley, D. E. Reactive Alkyne Complexes of Tantalum and Their Metallacyclization Chemistry: Models for Alkyne Cyclotrimerization by the Early Transition Metals. *Organometallics* **1988**, *7*, 2067−2069. (c) Smith, D. P.; Strickler, J. R.; Gray, S. D.; Bruck, M. A.; Holmes, R. S.; Wigley, D. E. Early-Transition-Metal-Mediated [2 + 2+2] Cycloadditions: Formation and Fragmentation of a Reactive Metallacyclopentadiene and Its Direct Conversion to $2^6$-Arene and $-^2$-Pyridine Complexes of Tantalum. *Organometallics* **1992**, *11*, 1275−1288. (d) Diercks, R.; Eaton, B. E.; Gürtzgen, S.; Jalisatgi, S.; Matzger, A. J.; Radde, R. H.; Vollhardt, K. P. C. The First Metallacyclopentadiene(Alkyne) Complexes and Their Discrete Isomerization to $\eta^4$-Bound Arenes: The Missing Link in the Prevalent Mechanism of Transition Metal Catalyzed Alkyne Cyclotrimerizations, as Exemplified by Cyclopentadienylcobalt. *J. Am. Chem. Soc.* **1998**, *120*, 8247−8248. (e) Wakatsuki, Y.; Yamazaki, H. Cobalt Metallocycles. *J. Organomet. Chem.* **1977**, *139*, 169−177. (f) Baxter, R. J.; Knox, G. R.; Moir, J. H.; Pauson, P. L.; Spicer, M. D. Formation of Arenes and of Tetracarbonyl(Hexatrienediyl)Dicobalt ("Flyover") Complexes from $Co_2(CO)_8$. *Organometallics* **1999**, *18*, 206−214. (g) Baxter, R. J.; Knox, G. R.; Pauson, P. L.; Spicer, M. D. Synthesis of Dicarbonyl($\eta^4$ -Tricarbonylcobaltacyclopentadiene)Cobalt Complexes from $Co_2(CO)_8$. A General Route to Intermediates in Cobalt Carbonyl Mediated Alkyne Trimerization. *Organometallics* **1999**, *18*, 197−205. (h) Dosa, P. I.; Whitener, G. D.; Vollhardt, K. P. C.; Bond, A. D.; Teat, S. J. Cobalt-Mediated Synthesis of Angular [4]Phenylene: Structural Characterization of a Metallacyclopentadiene(Alkyne) Intermediate and Its Thermal and Photochemical Conversion. *Org. Lett.* **2002**, *4*, 2075−2078. (i) Yamamoto, K.; Tsurugi, H.; Mashima, K. Direct Evidence for a [4 + 2] Cycloaddition Mechanism of Alkynes to Tantallacyclopentadiene on Dinuclear Tantalum Complexes as a Model of Alkyne Cyclotrimerization. *Chem. - Eur. J.* **2015**, *21*, 11369−11377. (j) Yamamoto, K.; Tsurugi, H.; Mashima, K. Alkyne-Induced Facile C-C Bond Formation of Two $u^2$-Alkynes on Dinuclear Tantalum Bis(Alkyne) Complexes to Give Dinuclear Tantalacyclopentadienes. *Organometallics* **2016**, *35*, 1573−1581.

(25) For examples of metallacyclopentatrienes, with delocalization of the $\pi$ electrons within the metallacycle, see: (a) Hirpo, W.; Curtis, M. D. A Folded Metallacyclopentatriene and a Bicapped-Tetrahedral $M_2C_4$ Cluster Obtained from Coupling of Alkyne Ligands. Structures of $CpMoCl(C_4Ph_4)$ and $(CpMoCl)_2(\mu\eta^4\text{-}C_4Ar_4)$ (Ar = *p*-Tolyl). *J. Am. Chem. Soc.* **1988**, *110*, 5218−5219. (b) Hessen, B.; Meetsma, A.; Van Bolhuis, F.; Teuben, J. H.; Helgesson, G.; Jagner, S. Chemistry of Carbon Monoxide Free Monocyclopentadienylvanadium(I) Alkene and Alkyne Complexes. *Organometallics* **1990**, *9*, 1925−1936. (c) Pu, L.; Hasegawa, T.; Parkin, S.; Taube, H. Osmacyclopentatriene Complexes: Structural Characterization of $[Os(C_4Me_4)(En)_2]\text{-}(CF_3SO_3)_2$. *J. Am. Chem. Soc.* **1992**, *114*, 2712−2713. (d) Mereiter, K.; Schmid, R.; Kirchner, K. Reactivity of a Metallacyclopentatriene Intermediate: Metal-to-Ligand-to-Metal Re-Migration of a Phosphine Ligand versus a 1,2 Hydrogen Shift. *Chem. Commun.* **2001**, *80*, 1996−1997. (e) Ernst, C.; Walter, O.; Dinjus, E. Cp*Ru-Allylcarbene Complexes by Nucleophilic Attack of Cyclic Cp*Ru-Dicarbenes. *J. Organomet. Chem.* **2001**, *627*, 249−254. (f) Le Paih, J.; Monnier, F.; Dérien, S.; Dixneuf, P. H.; Clot, E.; Eisenstein, O. Biscarbene-Ruthenium Complexes in Catalysis: Novel Stereoselective Synthesis of (1*E*,3*E*) −1,4-Disubstituted-1,3-Dienes via Head-to-Head Coupling of Terminal Alkynes and Addition of Carboxylic Acids. *J. Am. Chem. Soc.* **2003**, *125*, 11964−11975. (g) Rosenthal, U.; Burlakov, V. V.; Arndt, P.; Baumann, W.; Spannenberg, A. Five-Membered Titana- and Zirconacyclocumulenes: Stable 1-Metallacyclopenta-2,3,4-Trienes. *Organometallics* **2005**, *24*, 456−471. (h) Liu, G.; Lu, X.; Gagliardo, M.; Beetstra, D. J.; Meetsma, A.; Hessen, B. Vanadium ($\beta$-



https://dx.doi.org/10.1021/acs.organomet.0c00172
*Organometallics* 2020, 39, 1998−2010

(Dimethylamino)Ethyl)Cyclopentadienyl Complexes with Diphenylacetylene Ligands. *Organometallics* **2008**, *27*, 2316−2320. (i) Albers, M. O.; De Waal, D. J. A.; Liles, D. C.; Robinson, D. J.; Singleton, E.; Wiege, M. B. The Novel Cyclodimerization of Phenylacetylene at a Ruthenium(II) Centre. The Synthesis and X-Ray Structural Characterization of the First Metallacyclopentatriene, [($^5$-$C_5H_5$)Ru-($C_4Ph_2H_2$)Br], and its Facile Conversion into Metallacyclopentadienes. *J. Chem. Soc., Chem. Commun.* **1986**, *22*, 1680−1682.

(26) *Chemical Bonds and Bond Energy*; Sanderson, R. T., Ed.; Academic Press: New York, NY, 1976.

(27) Thorn, D. L.; Hoffmann, R. Delocalization in Metallocycles. *Nouv. J. Chem.* **1979**, *2*, 39−45.

(28) For examples of 7-metallanorbornadienes, see refs 24c,i and: (a) Kang, J. W.; Childs, R. F.; Maitlis, P. M. Fluxional Behavior in Tetrahaptobenzene-Rhodium and -Iridium Complexes. *J. Am. Chem. Soc.* **1970**, *92*, 720−722. (b) Jonas, K.; Wiskamp, V.; Tsay, Y. H.; Krueger, C. Metal-Bridging Benzene in a Binuclear Hydridovanadium Complex. *J. Am. Chem. Soc.* **1983**, *105*, 5480−5481. (c) Bruck, M. A.; Copenhaver, A. S.; Wigley, D. E. Alkyne Cyclizations at Reduced Tantalum Centers: Synthesis and Molecular Structure of ($\eta^6$-$C_6Me_6$)Ta(O-2,6-*i*-$Pr_2C_6H_3$)$_2$Cl. *J. Am. Chem. Soc.* **1987**, *109*, 6525−6527. (d) Ozerov, O. V.; Patrick, B. O.; Ladipo, F. T. Highly Regioselective [2 + 2+2] Cycloaddition of Terminal Alkynes Catalyzed by $\eta^6$ -Arene Complexes of Titanium Supported by Dimethylsilyl-Bridged *p*-Tert -Butyl Calix[4]Arene Ligand. *J. Am. Chem. Soc.* **2000**, *122*, 6423−6431.

(29) For examples of $\eta^4$-bound benzene−metal complexes, see refs 24d,h and: (a) Kölle, U.; Fuss, B. Pentamethylcyclopentadienyl-Übergangsmetall-Komplexe. X. Neue Co-Komplexe Aus X$^5$-$C_5Me_5$Co-Fragmenten Und Acetylenen. *Chem. Ber.* **1986**, *119*, 116−128. (b) Bottari, G.; Santos, L. L.; Posadas, C. M.; Campos, J.; Mereiter, K.; Paneque, M. Reaction of [TpRh($C_2H_4$)$_2$] with Dimethyl Acetylenedicarboxylate: Identification of Intermediates of the [2 + 2+2] Alkyne and Alkyne-Ethylene Cyclo(Co)Trimerizations. *Chem. - Eur. J.* **2016**, *22*, 13715−13723.

(30) For examples of metallabicyclo[3.2.0]-heptatrienes, see: (a) Agh-Atabay, N. M.; Davidson, J. L.; Douglas, G.; Muirb, K. W. Metal-Promoted Alkyne Trimerisation Leading to Novel Metallacycles. The Molecular Structures of [Mo{$\eta^3$-C($CF_3$)C($CF_3$)C(Me) = C(Ph)SPr$^i$}($CF_3CCCCF_3$)($\eta^5$-$C_5H_5$)], [WSPr$^i$\{$\eta^5$-C($CF_3$)C($CF_3$)C-($CF_3$)=C($CF_3$)C(Me)=C(Ph)\} ($\eta^5$-$C_5H_5$)], and [W($SC_6H_4$Me-4)\{$\eta^4$-C($CF_3$)=C($CF_3$)C($CO_2$Me)=C($CO_2$Me)C($CF_3$)=C($CF_3$)\}-($\eta^5$-$C_5H_5$)]. *J. Chem. Soc., Chem. Commun.* **1989**, *61*, 549−551. (b) Paneque, M.; Poveda, M. L.; Rendón, N.; Mereiter, K. Isolation of a Stable 1-Iridabicyclo[3.2.0]Hepta-1,3,6-Triene and Its Reversible Transformation into an Iridacycloheptatriene. *J. Am. Chem. Soc.* **2004**, *126*, 1610−1611.

(31) For examples of metallacycloheptatrienes, see ref 30b and: (a) Browning, J.; Green, M.; Penfold, P. R.; Stone, J. L.; Spencer, F. G. A. Synthesis and Crystal Structure of Bis(Triethylphosphine)-[Hexakis-(Trifluoromethyl)Benzene]Platinum, and of a Nickelacycloheptatriene Complex. *J. Chem. Soc., Chem. Commun.* **1973**, 31−32. (b) Browning, J.; Penfold, B. R. Structural Studies of Low-Valent Metal-Fluorocarbon Complexes. III. Crystal and Molecular Structure of Bis(Trimethylphosphite)Nickelahexakis-(Trifluoromethyl) Cyclohepta-Cis, Trans, Cis-Triene Containing a Chelate Ring with $\pi$-Bonding. *J. Cryst. Mol. Struct.* **1974**, *4*, 347−356. (c) Calderazzo, F.; Pampaloni, G.; Pallavicini, P.; Straehle, J.; Wurst, K. Reactions of Zirconium(3$^6$-Benzene)($AlCl_4$)$_2$ with Alkynes: Cyclooligomerization Reactions and Crystal and Molecular Structure of the Seven-Membered Metallacycle [ZrCPh($CPh)_4$CPh][(C-Cl)$_2AlCl_2$]$_2$. *Organometallics* **1991**, *10*, 896−901. (d) Álvarez, E.; Gómez, M.; Paneque, M.; Posadas, C. M.; Poveda, M. L.; Rendón, N.; Santos, L. L.; Rojas-Lima, S.; Salazar, V.; Mereiter, K.; Ruiz, C. Coupling of Internal Alkynes in $TpMe_2$Ir Derivatives: Selective Oxidation of a Non-coordinated Double Bond of the Resulting Iridacycloheptatrienes. *J. Am. Chem. Soc.* **2003**, *125*, 1478−1479.

(32) All calculations were performed with: Frisch, M. J.; Trucks, G. W.; Schlegel, H. B.; Scuseria, G. E.; Robb, M. A.; Cheeseman, J. R.; Scalmani, G.; Barone, V.; Mennucci, B.; Petersson, G. A.; Nakatsuji, H.; Caricato, M.; Li, X.; Hratchian, H. P.; Izmaylov, A. F.; Bloino, J.; Zheng, G.; Sonnenberg, J. L.; Hada, M.; Ehara, M.; Toyota, K.; Fukuda, R.; Hasegawa, J.; Ishida, M.; Nakajima, T.; Honda, Y.; Kitao, O.; Nakai, H.; Vreven, T.; Montgomery, J. A.; Peralta, J. E.; Ogliaro, F.; Bearpark, M.; Heyd, J. J.; Brothers, E.; Kudin, K. N.; Staroverov, V. N.; Kobayashi, R.; Normand, J.; Raghavachari, K.; Rendell, A.; Burant, J. C.; Iyengar, S. S.; Tomasi, J.; Cossi, M.; Rega, N.; Millam, J. M.; Klene, M.; Knox, J. E.; Cross, J. B.; Bakken, V.; Amado, C.; Jaramillo, J.; Gomperts, R.; Stratmann, R. E.; Yazyev, O.; Austin, A. J.; Cammi, R.; Pomelli, C.; Ochterski, J. W.; Martin, R. L.; Morokuma, K.; Zakrzewski, V. G.; Voth, G. A.; Salvador, P.; Dannenberg, J. J.; Dapprich, S.; Daniels, A. D.; Farkas, Ö.; Foresman, J. B.; Ortiz, V.; Cioslowski, J.; Fox, D. J. *Gaussian 16, Revision A.03*; Gaussian, Inc.: Wallingford, CT, 2016.

(33) Zhao, Y.; Truhlar, D. G. A New Local Density Functional for Main-Group Thermochemistry, Transition Metal Bonding, Thermochemical Kinetics, and Noncovalent Interactions. *J. Chem. Phys.* **2006**, *125*, 194101.

(34) Grimme, S.; Antony, J.; Ehrlich, S.; Krieg, H. A Consistent and Accurate Ab Initio Parametrization of Density Functional Dispersion Correction (DFT-D) for the 94 Elements H-Pu. *J. Chem. Phys.* **2010**, *132*, 154104−154119.

(35) All NBO analyses were performed with: Glendening, E. D.; Badenhoop, J. K.; Reed, A. E.; Carpenter, J. E.; Bohmann, J. A.; Morales, C. M.; Landis, C. R.; Weinhold, F. *NBO 6.0*; Theoretical Chemistry Institute, University of Wisconsin: Madison, WI, 2013.

(36) Jmol: an Open-Source Java Viewer for Chemical Structures in 3D; http://www.jmol.org/ (accessed March 9, 2020).



https://dx.doi.org/10.1021/acs.organomet.0c00172
*Organometallics* 2020, 39, 1998−2010